LEONARDO GOMIDES VEIGA

INTERPLAY BETWEEN GEOMETRY AND TOPOLOGY ON A CONICAL QUANTUM DOT

Dissertação apresentada à Universidade Federal de Viçosa, como parte das exigências do Programa de Pós-Graduação em Física, para obtenção do título de *Magister Scientiae*.

Orientador: Winder Alexander de Moura Melo

VIÇOSA-MINAS GERAIS
2020

Ficha catalográfica elaborada pela Biblioteca Central da Universidade Federal de Viçosa - Campus Viçosa

T
V426i
2020

Veiga, Leonardo Gomides, 1995-
Interplay between geometry and topology on a conical quantum dot / Leonardo Gomides Veiga. – Viçosa, MG, 2020.
64 f. : il. (algumas color.) ; 29 cm.

Inclui apêndices.
Orientador: Winder Alexander de Moura Melo.
Dissertação (mestrado) - Universidade Federal de Viçosa.
Referências bibliográficas: f.61-64.

1. Pontos quânticos. 2. Isolantes topológicos. 3. Superfícies (Matemática) . I. Universidade Federal de Viçosa. Departamento de Física. Programa de Pós-Graduação em Física. II. Título.

CDD 22. ed. 537.622

LEONARDO GOMIDES VEIGA

INTERPLAY BETWEEN GEOMETRY AND TOPOLOGY ON A CONICAL QUANTUM DOT

Dissertação apresentada à Universidade Federal de Viçosa, como parte das exigências do Programa de Pós-Graduação em Física, para obtenção do título de *Magister Scientiae*.

APROVADA: 19 de fevereiro de 2020.

Assentimento:

Leonardo Gomides Veiga
Autor

Winder Alexander de Moura Melo
Orientador

Agradecimentos

Agradeço a todos que colaboraram, direta ou indiretamente, para a realização deste trabalho. Em especial, ao meu orientador Winder A. Moura-Melo pela oportunidade, aos meus amigos e à minha família. O presente trabalho foi realizado com apoio da Coordenação de Aperfeiçoamento de Pessoal de Nível Superior – Brasil (CAPES) – Código de Financiamento 001.

Resumo

VEIGA, Leonardo Gomides, M.Sc., Universidade Federal de Viçosa, fevereiro de 2020. **Interação entre topologia e geometria num ponto quântico cônico**. Orientador: Winder Alexander Moura Melo.

Este trabalho teve como objetivo o estudo da interação entre confinamento quântico e características topológicas em sistemas de matéria condensada com geometria complexa. Em particular, estudamos um ponto quântico cônico feito de um isolante topológico, onde a não-trivialidade local da ponta do cone (o cone tem curvatura nula em todo seu espaço exceto na ponta, onde há uma singularidade), pode levar a efeitos globais nos portadores de carga que residem na superfície. Começamos introduzindo um ponto quântico cônico ordinário (i.e, um semicondutor) através de um modelo efetivo para tal, e fazemos uma introdução à topologia em matéria condensada e isolantes topológicos. O operador de Dirac efetivo que atua nos portadores de carga na superfície do isolante topológico cônico é calculado, e a equação de Dirac que descreve a dinâmica desses portadores é resolvida por completo. Discutimos os efeitos geométricos e topológicos associados á singularidade e como a função de onda e o espectro de energia são afetados por esses efeitos.

Palavras-chave: Pontos quânticos. Isolantes topológicos. Confinamento quântico. Equação de Dirac em espaços curvos.

Abstract

VEIGA, Leonardo Gomides, M.Sc., Universidade Federal de Viçosa, February, 2020. **Interplay between geometry and topology on a conical quantum dot**. Advisor: Winder Alexander Moura Melo.

This work is aimed to the study of the interplay between quantum confinement and topological features in condensed matter systems with complex geometry. More specifically we studied a conical topological insulator quantum dot (CTIQD), where the local nontriviality of the cone tip (the cone has null curvature everywhere but at the tip, where there is a singularity) can lead to global effects in the surface charge carriers and its energies spectrum and properties. We start by introducing an ordinary conical quantum dot (i.e., a semiconductor) through an effective model , and we make an introduction to topology in condensed matter and topological insulators. The effective Dirac operator that acts on the charge carriers on the surface of the conical topological insulator is calculated, and the Dirac equation that describes the dynamics of these carriers is completely solved. We discussed the geometric and topological effects associated with the singularity and how the wave function and the energy spectrum are affected by these effects.

Keywords: Quantum dots. Topological insulators. Quantum confinement. Dirac equation on curved spaces.

Contents

Chapter 1

Introduction

As a branch of Physics, the 'condensed matter physics' proposes to study many-body systems that are in condensed states. In this kind of systems we deal with a incredible high number of particles (at the order of Avogadro's constant, 10^{23} particles) and so the physics describing this "new world" is an emerging physics that emerges from the combination of the fundamental physics describing each of these particles individually. In general we are interested on a quantum mechanical representation of systems that are much larger (in scale) than the individual atom's nano-metric range, typically in the range of micrometers. It is not a coincidence that this is the usual length scale of modern devices (and electronics in general): condensed matter physics is celebrated not only because of the emergency of new physics, but also because of the really important applications that changed our everyday life around the world.

In his acclaimed article "More Is Different" [1], P. W. Anderson provides a philosophical discussion on the scientific methods of the reductionism and its connection to condensed matter physics. Besides that, he also discuss the emergent physics on these many-particle systems and how it can be fundamentally different from the physics of the single particle. In fact, the interactions between the countless particles, atoms or molecules that make up the system can lead to collective modes that have their own elementary excitations (with its own charge, spin, etc.) and physical properties that are very different from those observed in the elementary particles. The simplest example of this behaviour are the phonons representing a vibration on a solid. The phonon is a particle associated to a wave that propagates on the solid and it is the result of a collective behaviour (from many and many particles that compose the solid).

Until the beginning of the 80's, almost all the states of matter were successful catego-

rized according to its ordered phases. It is due to Ginzburg and Landau the theory that states that each phase has a local order parameter, which is finite in the ordered phase and zero otherwise, and that phase transitions occur when there are symmetry breaking. For example, water freezing breaks translational symmetry, the transition between a paramagnet and a ferromagnet at the Curie temperature corresponds to the breaking of a rotational symmetry and the superconducting transition is associated to gauge symmetry breaking [2].

However, this classification of materials depending on the spontaneously broken symmetries had to be revisited after von Klitzing's et al. paper from 1980 on the integer quantum Hall effect[4]: there was now a new state of matter that wasn't inside the Ginzburg-Landau's theory scope. It involves no broken symmetries and the phase transition that leads to this materials are of a topological nature. This work represents the start of another branch in physics called 'topological states of matter', that are characterized by certain quantities which are topologically invariant, and because of that it has become an interesting part of condensed matter physics.

One of this topological states is the so called topological insulator (TI). Topological insulators are a new state of quantum matter that arises from the impossibility of an adiabatic connection between them and the conventional insulators/semiconductors and have the distinctive feature of being insulators at the bulk and conductors at the surface (more on topological insulators will be discussed on chapter 4). These surface states are quite amusing since they are chiral, counter-propagating (in the sense that opposite spin-state particles travels in opposite directions) and highly protected by time reversal symmetry (TRS) against non-magnetic impurities and perturbations. Also, the strong spin-orbit coupling in these systems bring about a spin-momentum locking (the carriers in the surface states have their spin locked at a right-angle to their momentum)[5]. That being said, it is natural to expect that topological insulators are good candidates for spintronics. There are a lot of other effects that emerges from these topological systems, such as the topological magneto-electric effect (TMEE), which consists in a magnetic (electric) response to an electric (magnetic) induction, and also the appearing of Majorana's fermions in topological superconductors systems, that are good contenders for quantum computing [6].

Interesting effects can appear when we (quantum) confine topological insulators into a small region of space. The study of quantum confined systems leads to another new

class of objects called quantum dots (QDs). The unique feature of these objects is the discreteness of its energy spectrum (see Figure 1.1), which emerges naturally from total spatial confinement (in all three dimensions), and because of this they are called "artificial atoms". Semiconductor based quantum dots, for example, are of great interest since the energy band gap (and so the emission/absorption spectrum) can be controlled tuning the size of the dot (see Figure 1.2). Based on this property, a variety of applications have been demonstrated for quantum dots, including tunable light emitting diodes (LEDs), photovoltaics, single-electron transistors and fluorescent tags for biological imaging applications [7].

Figure 1.1: Schematic illustration of the energy levels of a bulk 3d semiconductor and of semiconductor nanostructures with reduction in dimensionality, being the 2d named "quantum well", 1d named "quantum wire" and the 0d "quantum dot". Basically, the state density by energy curve indicates the number of states available by energy level. Note that as we reduce dimensionality, the continuity of these available states are no more, i.e, only a few energy states are allowed.

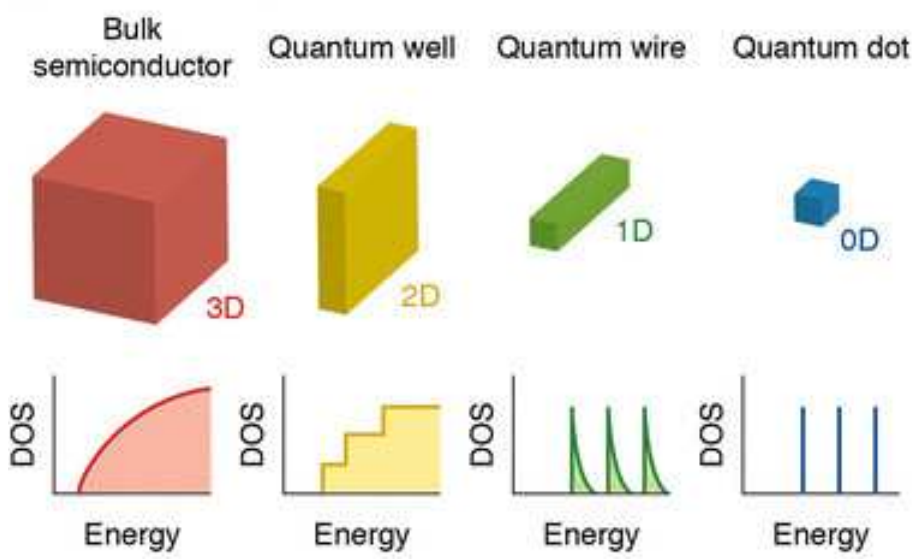

Source: https://link.springer.com/content/pdf/10.10072Fs41061-016-0060-0.pdf.

The unique signature of the quantum dots (discrete energy levels) can be reproduced in topological insulators by a process of miniaturization. From this process arise the topological insulator quantum dots (TIQD) or the topological insulator nano-particles (TINP). This is a relatively new branch of physics, and some studies conclude that topological insulators can be miniaturized until about 10 nm without the opening of a gap at the surface [8],[9]. This robustness against surface states hybridization are important to quantum computing and other nano-scale applications.

It is known that the the surface states in a topological insulator with preserved TRS are described by a Dirac-like equation for massless fermions. If we are dealing with a curved geometry, we must couple the Dirac equation to the coordinate system and this can lead to interesting phenomena. In fact, it has been shown that the connections for a curved Dirac equation act like an effective potential, contributing effectively to the dynamics [10]. In this context, one can think of conical geometry as it is a peculiar choice because of the non-triviality of its tip. From a differential geometry point of view, the cone has a null Gaussian curvature at all points, except at the tip where there is a singularity. The question that arises is whether the local nontriviality of the cone tip can generate global effects, and this question was explored on [3], where it was shown a geometrically induced (by the singularity at the tip) electric polarization depending only on the apex angle of the cone, for a conical topological insulator.

Figure 1.2: Energy level due to quantum confinement effect. The semiconductor gap increases with decreasing nano-crystal size and therefore we have a blue shift. In addition, we note the discreteness in the energies of the quantum dots when compared to bulk.

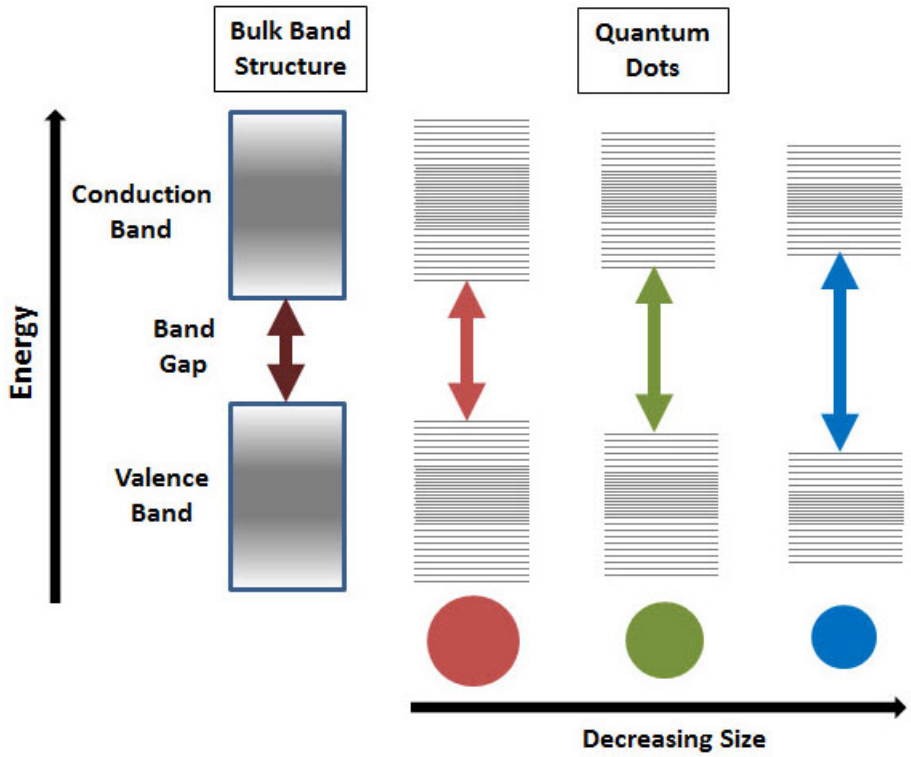

Source: https://www.sigmaaldrich.com/technicaldocuments/articles/materials-science/nanomaterials /quantum-dots.html.

Based on the discussion above, we organized a dissertation that is aimed to the study of the interplay between quantum confinement and topological features in condensed matter

systems with complex geometry. More specifically, we will study a conical topological insulator quantum dot (CTIQD), where the local non-triviality of the cone tip (the cone has null curvature everywhere but at the tip, where there is a singularity) can lead to global effects in the surface charge carriers and its energies spectrum and properties.

Chapter 2

The conical quantum dot

2.1 A simplified approach for semiconductors quantum dots

The states of an ideal crystal are formally described by the eigenstates of the following Hamiltonian:

$$H = \sum_i \frac{p_i^2}{2m_i} + \sum_I \frac{p_I^2}{2m_I} + \frac{1}{2}\sum_{I<J} \frac{Z_I Z_J e^2}{4\pi\epsilon_0 |\mathbf{R}_I - \mathbf{R}_J|} - \\ - \sum_{I,i} \frac{Z_I e^2}{4\pi\epsilon_0 |\mathbf{R}_I - \mathbf{r}_i|} + \sum_{i<j} \frac{e^2}{4\pi\epsilon_0 |\mathbf{r}_i - \mathbf{r}_j|} + H_s \quad , \quad (2.1)$$

where we explicitly account for the interactions between electrons and nuclei. We can reduce this cumbersome problem to a very simple one-electron problem by means of some approximations. We consider that the nuclei are approximately at rest compared to the electrons, and that these electrons experience a mean electrostatic field that is a combination of the fields of all the charge carries in the material. Each electron then is governed by a Bloch Hamiltonian (see Appendix A) and each state is determined by

$$H_e \psi_{n,k}(\mathbf{r}) = \left(\frac{\hat{p}^2}{2m} + V(\mathbf{r}) \right) \psi_{n,k}(\mathbf{r}) = E_n \psi_{n,k}(\mathbf{r}) \quad . \quad (2.2)$$

Now, in the effective mass approximation, we consider that near the energy gap the dispersion relation is parabolic, and the details of the band structure and its interactions are included in a effective mass term. The Hamiltonian now is governed by a confinement potential, and we can add other interactions (Coulomb, spin-orbit..) with perturbation

methods. If we are talking about a confinement potential that trap particles in a very small region (to the order of de Broglie wavelength) so we have a quantum dot.

In general, quantum dots are classified in three classes depending on its size (compared with the Bohr radius associated with the charge carriers): the strong confinement, the intermediate confinement and the weak confinement. In the strong confinement (for particles with radius smaller than the Bohr radius) we can assume that the electrons and holes' motions are individually quantized, so we can solve its motions separately. It is somewhat simpler to work on the strong confinement limit, and for our purposes (to see the geometrical effects on quantum dots) it may be adequate. It is quite common to use the infinite mass boundary condition (infinite confinement potential) to treat quantum dots on the strong confinement, but it is known that this approach is not to be fully trusted [40]. Although, for simplicity, we will assume the infinite mass boundary condition when talking about the semiconductor conical quantum dot.

2.2 Conical geometry

The cone has null curvature and torsion at all points on its surface except at the tip, where it has a singularity. Thus, with the exception of the apex point, the surface of a cone can be described by spherical coordinates, where we realize that a constant polar angle leads to a conical surface, as illustrated in Figure 2.1

Identifying the coordinates $x_1 = r, x_2 = \phi, x_3 = \theta$, the tangent surface vectors are defined as

$$\mathbf{e}_i = \frac{\partial \mathbf{x}}{\partial x_i} \text{ where } i = 1, 2 \quad ,$$

and the normal surface vector is:

$$\mathbf{e}_3 = \frac{\mathbf{e}_1 \times \mathbf{e}_2}{|\mathbf{e}_1 \times \mathbf{e}_2|} \quad .$$

Now, using the spherical coordinate position vector $\mathbf{x} = (r\sin\theta\cos\phi, r\sin\theta\sin\phi, r\cos\theta)$, where $\theta = \text{cte}$, we get

$$\begin{aligned}
\mathbf{e}_1 &= (\sin\theta\cos\phi,\ \sin\theta\sin\phi,\ \cos\theta) \\
\mathbf{e}_1 &= (-r\sin\theta\sin\phi,\ r\sin\theta\cos\phi,\ 0) \\
\mathbf{e}_3 &= (-\cos\theta\cos\phi,\ \cos\theta\sin\phi,\ \sin\theta) \quad .
\end{aligned}$$

Figure 2.1: In the usual spherical coordinates, a cone is generated fixing the polar angle. The radial coordinate is the generating line of the cone.

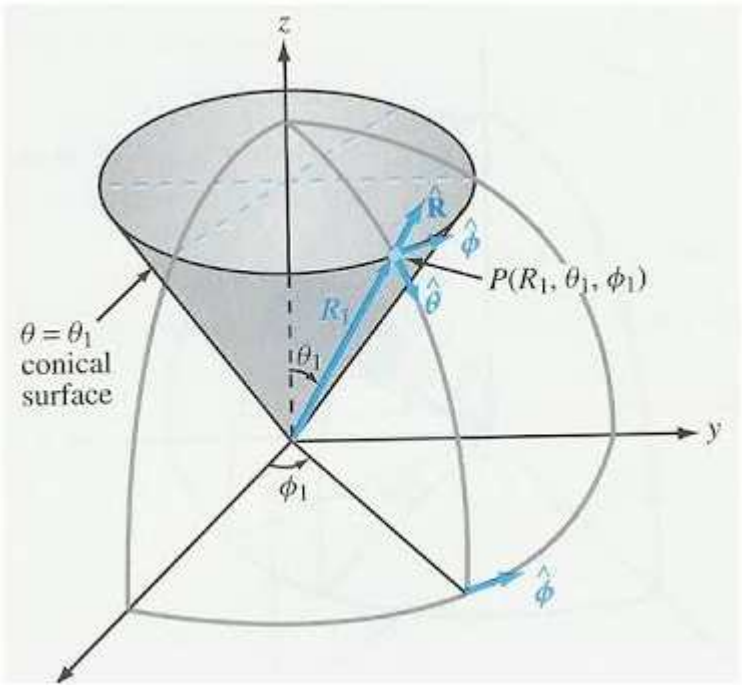

To simplify the notation, we will adopt the identifications $\sin\theta \equiv a$, $\cos\theta \equiv b$. In order to find the metric tensor we define $\mathbf{e}^i$ such as $\mathbf{e}_i \cdot \mathbf{e}^j = \delta_{ij}$, then the metric is defined as $g_{ij} \equiv \mathbf{e}_i \cdot \mathbf{e}_j$, with inverse $g^{ij} \equiv \mathbf{e}^i \cdot \mathbf{e}^j$. The metric tensor for the points at the surface will be:

$$\begin{bmatrix} 1 & 0 \\ 0 & r^2 a^2 \end{bmatrix}, \tag{2.3}$$

with $\sqrt{G} = ra$. These identifications will be important to couple the Dirac operator to the coordinate system when talking about the conical topological insulator. Also, it is worth mention the following relations:

$$R^2 = h^2 + R'^2 \quad ;$$

$$\frac{a}{b} = \frac{R'}{h} \quad ;$$

$$b = \frac{h}{R} \quad \rightarrow \quad R = hb^{-1} \quad ;$$

$$\text{Volume} = \frac{\pi R'^2 h}{3} \quad ,$$

where R' is the radius of the cone's basis, R is the generating line in the radial direction and h is the cone's height.

Another way to construct a cone is to remove a sector γ from a sheet. The identification of the edges lead to a cone with the same metric.

Figure 2.2: Removal of a γ sector from the bi-dimensional Euclidian space and the identification of the edges leading to a cone. The apex angle and the sector removed are linked by $\sin\beta = 1-\gamma$

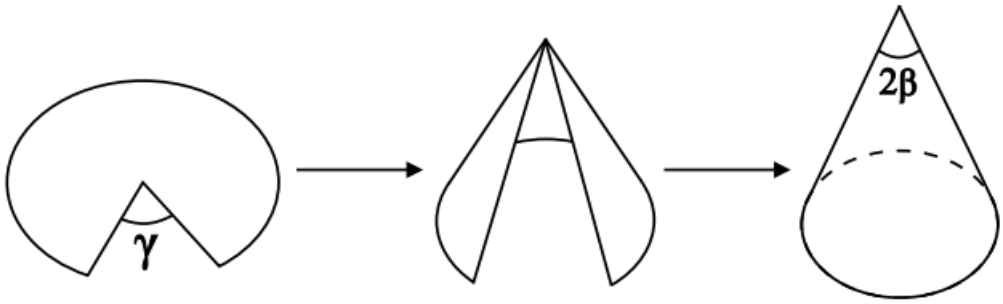

Source: reference [35].

2.3 Electronic properties of the conical quantum dot

We will extent the discussion made on [43]. Working on the effective mass approximation, we assume a infinite potential for the confinement:

$$V_{\text{conf}} = \begin{cases} 0, & \text{inside} \\ \infty, & \text{outside} \end{cases} \quad , \tag{2.4}$$

and our problem is to solve the Helmholtz equation:

$$\nabla^2\psi + k^2\psi = 0 \quad . \tag{2.5}$$

where $k^2 = \frac{\sqrt{2mE}}{\hbar}$. As said in the last section, we'll work on spherical coordinates, in such a way that the range of the coordinates are $r \leq R$, $0 \leq \phi \leq 2\pi$, $\theta \leq \alpha = \text{cte}$.

The solutions are given by

$$\psi(r,\theta,\phi) = CR(r)\Theta(\theta)e^{im\phi} \quad . \tag{2.6}$$

The solution of the angular equation $\Theta(\theta)$ is the associated Legendre polynomials $P_l^m(\cos\theta)$, where the non-trivial conical boundary condition turn the index l into a real number (remember that in usual spherical symmetric problems l is integer). The solution of the

radial problem is the spherical Bessel function, and we have:

$$\psi(r,\theta,\phi) = C\mathcal{J}_l(kr)P_l^m(\cos\theta)\,e^{im\phi} \quad , \tag{2.7}$$

which has the same shape of the spherical hard-wall text book problem. However we have here two confinements: one in the radial direction and other in the polar direction (that defines the constant conical surface). The wavefunction must vanish on $r = R$ (i.e, the cone has a finite size) and on $\theta = \alpha$,

$$P_l^m(b) = 0 \rightarrow l = l_{mi}$$
$$j_l(kR) = 0 \rightarrow \mathcal{J}_{l_{mi}}(kR) = 0 \rightarrow k = \frac{\beta_{l_{mi},n}}{R} \quad ,$$

where l_{mi} is the ith zero of the associated Legendre function of order m (m is integer to ensure a single-valued azimuthal function), and $\beta_{l_{mi},n}$ is the nth zero of the spherical Bessel function of order l_{mi}. The energies are

$$E_{n,i,m} = E_g + \frac{\hbar^2}{2\mu^*}\frac{\beta_{l_{mi},n}^2}{h^2 b^{-2}} \quad , \tag{2.8}$$

with μ being the effective reduced mass $\left(\frac{1}{m_e^*} + \frac{1}{m_h^*}\right)$ of the pair electron-hole. We can plot the energies in function of different geometrical parameters:

Figure 2.3: Energy plotted in function of the cone height for various apex angles α. The lower the apex angle, the greater the energy due to confinement (for the same height). For large radius, the energy goes asymptotically to the gap energy.

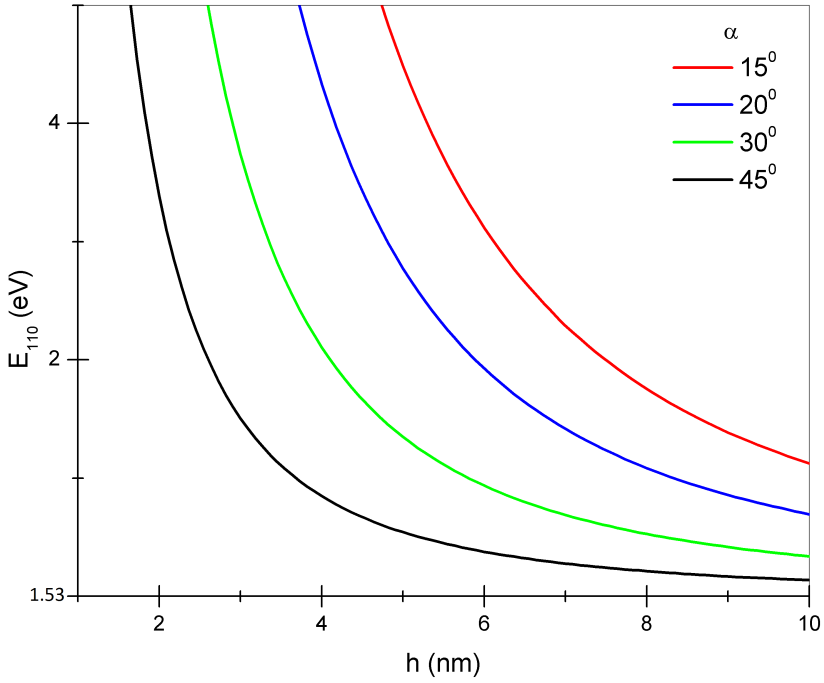

Figure 2.4: Energy plotted in function of the basis radius for various apex angles α. For a fixed radius, the lower the apex angle, the lower the energy.

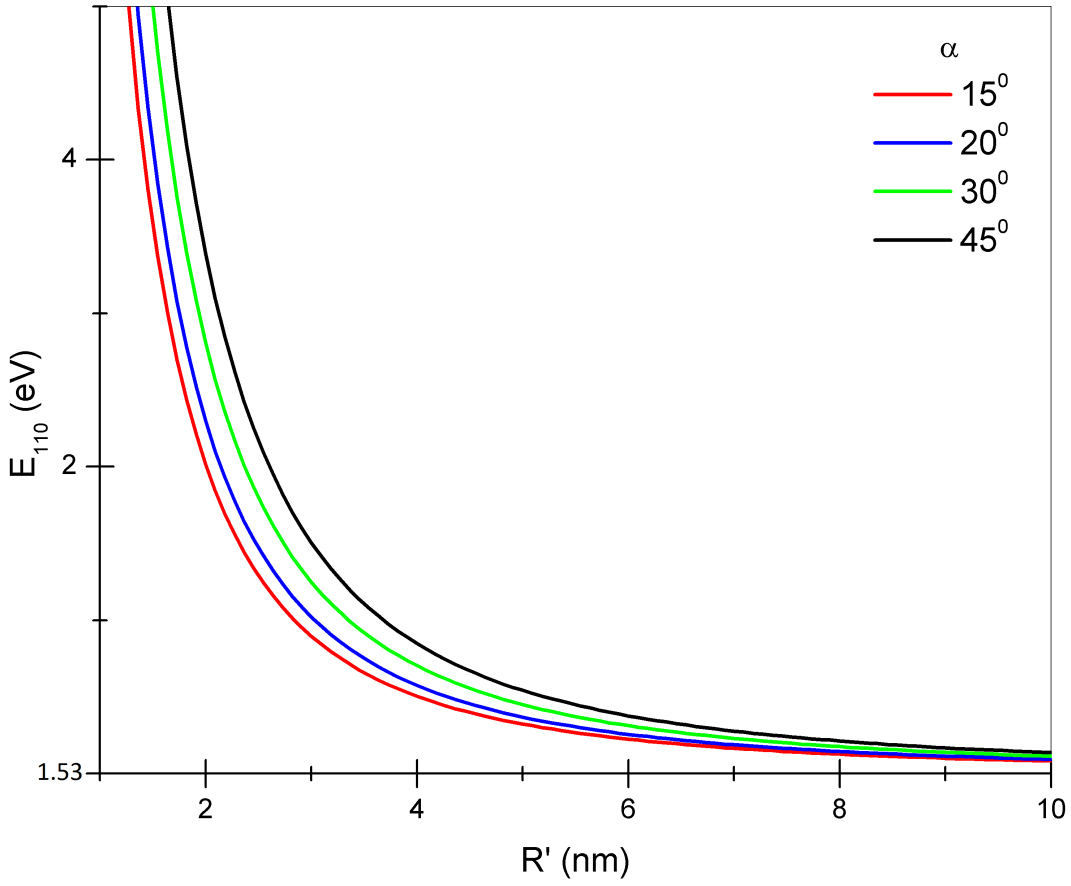

Apparently, the decisive quantity on the quantum confinement is the volume of the region. The conical volume is defined by a set of two independent parameters (e.g. the basis radius and the height) and since it depends differently on each parameter (it depends on the square of the basis radius, while it is linear in the height) we get different energies when we fix each of these parameters. We can compare the energies for the same volume for different geometries. The solutions for the spherical and the cylindrical quantum dots in this context are well known, and the Figure 2.5 illustrate this comparison.

The interesting result here is that keeping the same volume for a quantum dot (that is, maintaining the amount of material for the production of such), but by varying its geometric parameters, it is possible to produce quantum dots with different energies. Since a lot of properties like the absorption coefficient depends directly on the energy dispersion, we can choose a geometry (without changing the total volume) that creates a desired absorbtion/emission peak.

Figure 2.5: Comparative graph of the ground state energy due to quantum confinement for spherical, cylindrical and conical quantum dots, for different volume values.

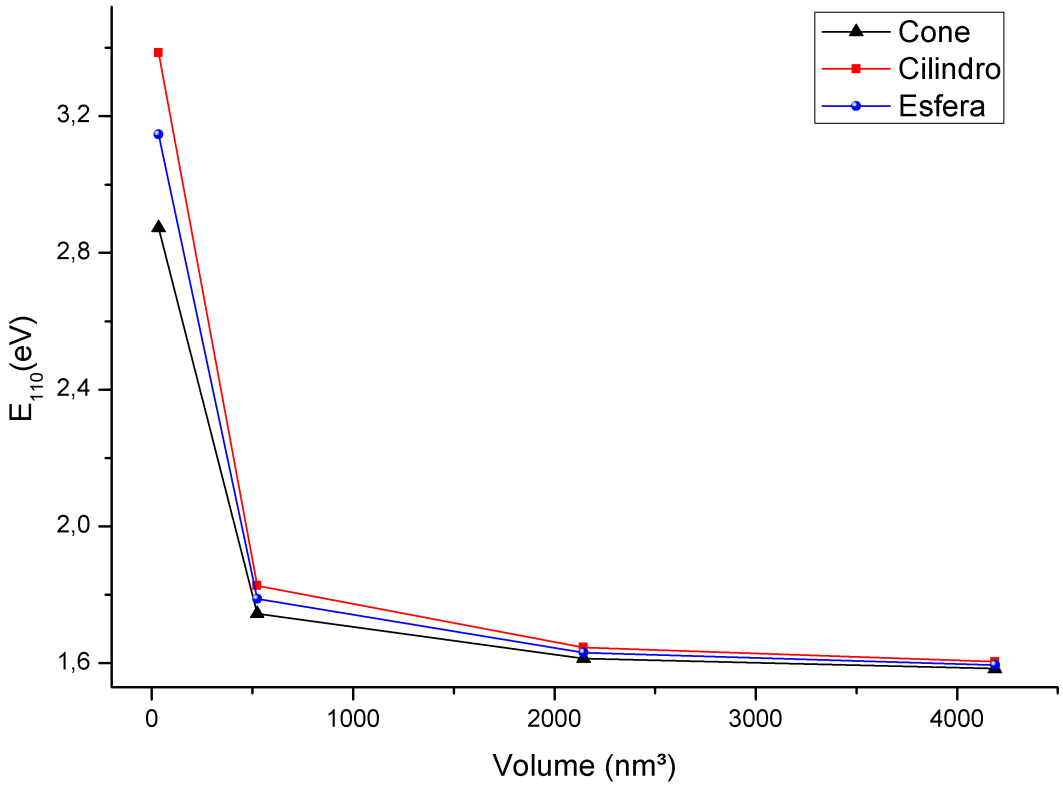

We will turn our discussion now to the topological version of this problem, but before we will briefly introduce some aspects of topological insulators.

Chapter 3

Basic aspects of 3D Topological Insulators

The topological insulators are a new class of insulators that are characterized by its non-trivial topological order, which produce conducting surface states. Thus, they are fundamentally different from ordinary insulators (which cannot conduct anywhere) and there are several interesting properties associated with this new class of materials. These metallic surface states are protected by time-reversal symmetry, and so they are robust against non-magnetic impurities. Due to strong spin-orbit coupling in these materials, the edge states exhibit the spin-to-momentum locking, where spin is always locked at right angles to the momentum, and both lying on the surface plane (to understand how these surface states appears and how it is related to topology, see Appendices A-C). To describe them, we will use the celebrated model developed by Bernevig, Hughes and Zhang.

3.1 The BHZ model

The BHZ effective Hamiltonian is essentially an k wave vector expansion in Taylor series of the interactions near the energy gap. Explicitly in 3D, this model reads:

$$H(\mathbf{k}) = \epsilon(\mathbf{k}) \cdot \mathbf{1_{4x4}} + \begin{pmatrix} M(\mathbf{k}) & Ak_z + & 0 & \tilde{A}k_- \\ Ak_z & -M(\mathbf{k}) & \tilde{A}k_- & 0 \\ 0 & \tilde{A}k_+ & M(\mathbf{k}) & -Ak_z \\ \tilde{A}k_+ & 0 & -Ak_z & -M(\mathbf{k}) \end{pmatrix}, \tag{3.1}$$

where $M_0(\mathbf{k}) \rightarrow M(\mathbf{k}) = M - B(k_x^2 + k_y^2 + k_z^2)$.. The parameters are determined by the details of each material. The mechanism from which the topological nature arise is called band inversion, and the condition for a (strong) topological phase is given by $\frac{M}{B} > 0$ (see Appendix C). If $\frac{M}{B} < 0$ it is a trivial phase, or an ordinary insulator.

In order to study the conducting edge states we project the Hamiltonian above onto the material surface, to get the following effective Hamiltonian (see equation C.11):

$$H_{sur} = -i\hbar v_F \boldsymbol{\sigma} \cdot \boldsymbol{\nabla} \quad , \tag{3.2}$$

where the Pauli matrices are correlated to the actual spin of surface states. The Hamiltonian above is a massless Dirac-like Hamiltonian. Thus the surface states of the three-dimensional TI described by equation above have a linear spectrum.

3.2 Quantum confined topological insulators

To talk about the interplay between topological insulators and quantum confinement, the fundamental question, considering that the topological properties discussed earlier arises from bulk properties, is whether there is enough bulk in a topological nanoparticle. In general, the surface states on a topological insulator are exponentially localized at the edge, i.e, they have a penetration length in the bulk, and when the spacing between the edges of a material is small enough, a gap become measurable due to the hybridization of the surface states.

It was shown in references [8],[9] that the surface states of some topological insulators, specially Bi_2Se_3, display a remarkable robustness towards finite size effects, becoming measurably gapped only when the bulk diameter drops to a few nm. Thus, it is possible to construct quantum dots made of topological insulators.

This system was studied by Imura et al. in reference [18], where a spherical topological insulator was considered and good agreement of the results with tight binding calculations suggests that the model was applicable to topological insulator nanoparticles. They showed that for this topological dots, the spectrum of surface states is not continuous but discrete, in such a way that the signature of quantum dots is printed in the nanoparticles, with the addition of protected delocalized surface states, that are robust to non-magnetic perturbations, which are the signatures of topological insulators. This combination of effects (see Figure 3.1) put topological nanoparticles in priority when

we talk about quantum computing and nanophotonics [19].

In fact, Siroki et al. reported in reference [20] that for a spherical quantum dot under the influence of light, a single electron in a topologically protected surface state creates a anomalous surface charge density similar that can act as a screening layer, which suppresses absorption inside the particle. In addition, it can couple phonons and light, giving rise to a previously unreported topological particle polariton mode.

Figure 3.1: Properties of topologically protected surface states. (a) Momentum and spin are locked. (b) Time-reversal symmetry avoids backscattering. (c) The signature of quantum confinement is the Dirac cone of a planar surface (green) turning into discrete states in nanoparticles (red dots). (d) The discrete states also cannot backscatter and are also protected from disorder as their continuous counterparts.

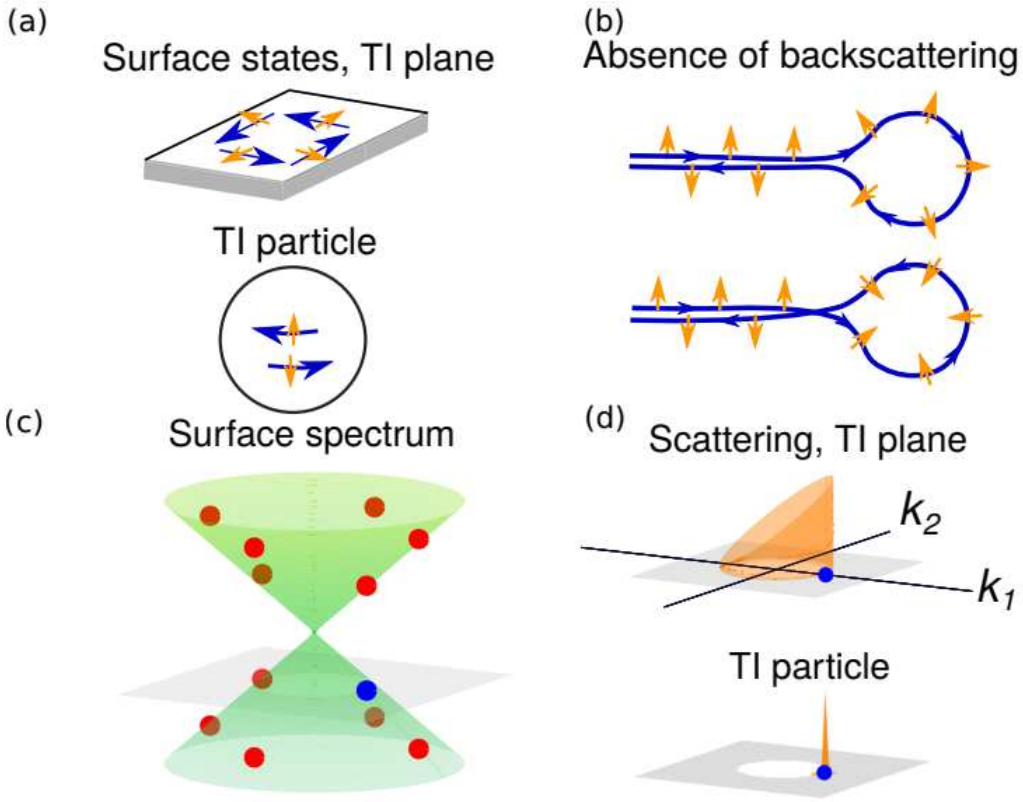

Source: Reference [9]

As a last remark on the miniaturization of topological insulators, in reference [21] the author demonstrated that, due to quantum confinement, quantum dots made of trivial BHZ insulators can display topological features such as helical spin-momentum locked protected (against non-magnetic perturbation) states, with high conductance similarly to a non-trivial topological insulator.

Chapter 4

The conical topological insulator quantum dot

4.1 The surface Dirac operator

The choice of the conical geometry was motivated by a work [3] which showed that the local nontriviality (in a geometrical point of view) of the cone tip can generate global effects on the charge carriers on a TI. In particular, on the surface of a conical topological insulator covered with a magnetic film (here the $\mathcal{T}$ symmetry is broken and the topological magnetoelectric effect plays a substancial role, see reference [5]), a geometrically induced (by the singularity at the tip) electric polarization depending only on the apex angle of the cone arises when a charge is brought to the neighbourhood of the cone. In this work we will talk about a conical topological insulator with time-reversal symmetry preserved.

We start by the BHZ model for a strong, isotropic 3D TI in the continuum limit

$$H(\mathbf{k}) = \epsilon(\mathbf{k}) \cdot \mathbf{1_{4x4}} + \begin{pmatrix} M(\mathbf{k}) & Ak_z + & 0 & Ak_- \\ Ak_z & -M(\mathbf{k}) & Ak_- & 0 \\ 0 & Ak_+ & M(\mathbf{k}) & -Ak_z \\ Ak_+ & 0 & -Ak_z & -M(\mathbf{k}) \end{pmatrix}, \tag{4.1}$$

where, to fix notation we set $M(\mathbf{k}) = m_0 + m_2(k_x^2 + k_y^2 + k_z^2)$. For simplicity, we choose $\epsilon(\mathbf{k})$ to be null in order for the spectrum to be symmetric with respect to $E = 0$. The vanishing of this term leaves unchanged the distinction between topologically trivial ($\frac{m_0}{m_2} > 0$) and nontrivial ($\frac{m_0}{m_2} < 0$) phases [22]. The isotropic condition together with the vanishing of

$\epsilon(\mathbf{k})$ led to a model with only three control parameters (A, m_0, m_2) [22]. From now on we set $\hbar = 1$, since our goal is to study the contribution from the nontrivial geometry of the system.

Now, following the BHZ development, we aim to project the bulk Hamiltonian onto the surface and to do this we rewrite Hamiltonian (4.1) in terms of the curvilinear coordinates, and then divide it into two components, one being perpendicular and the other tangent to the surface. The first part describes the penetration of the surface wave functions into the bulk, and the second part determine the energy properties of the surface. We have $H = H_\perp + H_\parallel$, with

$$H_\perp = \begin{bmatrix} m_0 - m_2\nabla_\perp^2 & -iA\sigma^3\partial_3 \\ -iA\sigma^3\partial_3 & -m_0 + m_2\nabla_\perp^2 \end{bmatrix}, \tag{4.2}$$

$$H_\perp = \begin{bmatrix} -m_2\nabla_\parallel^2 & -iA\sum_{i=i}^{2}\sigma^i\partial_i \\ -iA\sum_{i=i}^{2}\sigma^i\partial_i & m_2\nabla_\parallel^2 \end{bmatrix}, \tag{4.3}$$

where the laplace operators coupled to the conical geometry are read as $\nabla_\perp^2 = \frac{1}{\sin\theta}\partial_\theta(\sin\theta\partial_\theta)$, $\nabla_\parallel^2 = \frac{1}{r\sin\theta}\sum_{i,j=i}^{2}\partial_i(r\sin\theta g^{ij}\partial_j)$ [22]. Also, the spin matrices coupled to the coordinates are $\sigma^i \equiv \boldsymbol{e}^i \cdot \boldsymbol{\sigma}$, and for the conical geometry they read (remember that $\sin\theta \equiv a$, $\cos\theta \equiv b$):

$$\sigma^1 = \begin{bmatrix} b & -ae^{-i\phi} \\ ae^{i\phi} & -b \end{bmatrix}, \tag{4.4}$$

$$\sigma^2 = \frac{1}{ar}\begin{bmatrix} 0 & -ie^{-i\phi} \\ ie^{i\phi} & 0 \end{bmatrix}, \tag{4.5}$$

$$\sigma^3 = \begin{bmatrix} a & -be^{-i\phi} \\ -be^{i\phi} & -a \end{bmatrix}. \tag{4.6}$$

From now on, the details will be left in the Appendix D. In the the normal eingenvalue problem, we have

$$H_\perp|\psi\rangle = E_\perp|\psi\rangle \quad , \tag{4.7}$$

for which we can assume that the states are exponentially localized near the surface states:

$$|\psi\rangle = e^{k_-(\theta-\theta_0)}|u_-(r,\phi)\rangle - e^{k_+(\theta-\theta_0)}|u_+(r,\phi)\rangle \quad . \tag{4.8}$$

The proper boundary condition $|\psi(\theta=\theta_0)\rangle = 0$, which states that all four components of the wave function vanish on the surface of the cone (at $\theta=\theta_0$) and ensures that there are no charge carriers outside the TI surface, leads to a zero-energy condition and we find the $H_\perp$ basis eigenstates:

$$|\pm\rangle = \rho(\theta)\frac{1}{\sqrt{2}}\begin{bmatrix} |\boldsymbol{\theta}_+\rangle \\ \mp i|\boldsymbol{\theta}_-\rangle \end{bmatrix}, \tag{4.9}$$

with $\rho(\theta)$ being a linear combination of the exponentials and the vectors $|\boldsymbol{\theta}_+\rangle, |\boldsymbol{\theta}_-\rangle$ are eigenvectors of σ^3, satisfying

$$\sigma^3|\boldsymbol{\theta}_\pm\rangle = \pm|\boldsymbol{\theta}_\pm\rangle. \tag{4.10}$$

If we require that $|\boldsymbol{\theta}_\pm\rangle$ are connected by time-reversal as $|\boldsymbol{\theta}_+\rangle = -i\sigma_y|\boldsymbol{\theta}_-\rangle^*$, then we have for the conical geometry

$$|\boldsymbol{\theta}_+\rangle = \begin{bmatrix} -(a+1)e^{-i\frac{\phi}{2}} \\ be^{i\frac{\phi}{2}} \end{bmatrix}, \tag{4.11}$$

$$|\boldsymbol{\theta}_-\rangle = \begin{bmatrix} be^{-i\frac{\phi}{2}} \\ (a+1)e^{i\frac{\phi}{2}} \end{bmatrix}. \tag{4.12}$$

With all of these definitions, and noting that any surface state $|\psi\rangle$ can be represented as a linear combination of $|+\rangle$ and $|-\rangle$ as

$$|\psi\rangle = a_+|+\rangle + a_-|-\rangle \quad , \tag{4.13}$$

the effective surface Hamiltonian for the spinor $\boldsymbol{a} = \begin{bmatrix} a_+ \\ a_- \end{bmatrix}$, is specified as

$$H_{suf} = \begin{bmatrix} \langle +|H_\parallel|+\rangle & \langle +|H_\parallel|-\rangle \\ \langle -|H_\parallel|+\rangle & \langle -|H_\parallel|-\rangle \end{bmatrix} \quad . \tag{4.14}$$

The approach here is in parallel with that of the degenerate perturbation theory, as pointed out in [18]. Here, $H_0 = H_\perp$ is an unperturbed Hamiltonian and $|\pm\rangle$ are its degenerate eigenstates. To find the spectrum of the perturbed Hamiltonian $H_{tot} = H_0 + H'$, in which $H' = H_\parallel$ and $H_{tot} = H_{bulk}$, we have to calculate the matrix elements $\langle\alpha|H'|\beta\rangle$, $(\alpha,\beta=\pm)$ first, and then diagonalize it. After some cumbersome procedure, we find the surface

Dirac operator as

$$H_{sur} = \begin{bmatrix} 0 & \mathcal{D}_+ \\ \mathcal{D}_- & 0 \end{bmatrix}, \tag{4.15}$$

where

$$\mathcal{D}_\pm = \mp A\left(\frac{\partial}{\partial r} + \frac{1}{2r}\right) + \left(\frac{iA}{ar} + \frac{ib}{a^2r^2}m_2\right)\frac{\partial}{\partial \phi}. \tag{4.16}$$

Some comments can be made on this result. The first one is that the coupling $\partial_r \to \partial_r + \frac{1}{2r}$ is expected and it arises in theories for Dirac equation for curved surfaces [23]. It is related to the the spin connection, which couples the Dirac equation to a curved space. Also, a common path for solving surface states for 3D topological insulators is to build the Dirac operator for a flat surface and then implement the curved nature of a surface through a coordinate transformation, and in this approach the other terms relating the apex angle and the renormalization of the effective velocity arising from the m_2 term do not appear. This is because the "pure-2D" approach ignores the three dimensional nature of the problem [22], so you end up losing some information in the process. The second one is that the terms on the $\partial\phi$ operator can be viewed like "Aharanov-Bohm" potentials. The non-trivial curvature of the cone generate a effective Aharanov-Bohm flux that affects the system globally. This is a known effect in cosmology and particle physics [39].

4.2 The surface states and energies

In order to find the surface states and its energies, we must solve

$$H|\boldsymbol{\alpha}\rangle = E|\boldsymbol{\alpha}\rangle \to \begin{bmatrix} 0 & \mathcal{D}_+ \\ \mathcal{D}_- & 0 \end{bmatrix}\begin{bmatrix} \alpha_+(r,\phi) \\ \alpha_-(r,\phi) \end{bmatrix} = E\begin{bmatrix} \alpha_+(r,\phi) \\ \alpha_-(r,\phi) \end{bmatrix}. \tag{4.17}$$

Since the Hamiltonian above comute with the total angular momentum of a 2D Dirac system

$$\mathcal{J} = -i\frac{\partial}{\partial\phi} + \frac{1}{2}\sigma_z \quad , \tag{4.18}$$

we write the surface states as eigenfunctions of $\mathcal{J}$ with eigenvalues $j + \frac{1}{2}$, and they assume the form:

$$|\boldsymbol{\alpha}\rangle = \begin{bmatrix} u(r) \\ iv(r) \end{bmatrix} e^{i\phi(j+\frac{1}{2}+\frac{1}{2}\sigma_z)} = \begin{bmatrix} u(r)e^{i\phi j} \\ iv(r)e^{i\phi(j+1)} \end{bmatrix}, \tag{4.19}$$

At a first approximation, we neglect the $\frac{ib}{a^2r^2}m_2$ term. Applying the Dirac operator on this state, we get the following coupled differential equations

$$\begin{cases} -iA\left(\partial_r + \frac{1}{2r}\right)v(r) - \frac{iA(j+1)}{ar}v(r) = Eu(r) \\ A\left(\partial r + \frac{1}{2r}\right)u(r) - \frac{Aj}{ar}u(r) = iEv(r) \end{cases}$$

The equations above may be decoupled at second order leading to two Bessel-like equations:

$$r^2\frac{d^2v(r)}{dr^2} + r\left(1+\frac{1}{a}\right)\frac{dv(r)}{dr} + \left(r^2k^2 - \lambda_{j+}^2\right)v(r) = 0 \quad , \tag{4.20}$$

$$r^2\frac{d^2u(r)}{dr^2} + r\left(1+\frac{1}{a}\right)\frac{du(r)}{dr} + \left(r^2k^2 - \lambda_{j-}^2\right)u(r) = 0 \quad , \tag{4.21}$$

where $k^2 = \frac{E^2}{A^2}$ and $\lambda_{j\pm}^2 = \frac{j(j+1)}{a^2} \pm \frac{j}{a} \pm \frac{1}{2a} + \frac{1}{4}$.

We have a two-component spinor solution for positive and negative energies each, but since the $-E$ solutions are the mirror solutions of E, we focus only on the positive energies here. The two Bessel-like equations above can be transformed in the Bessel equation with the following identification:

$$\begin{bmatrix} u(r) \\ v(r) \end{bmatrix} \to r^{-\frac{1}{a}} \begin{bmatrix} u(r) \\ v(r) \end{bmatrix}. \tag{4.22}$$

With this identification, the solutions of the radial component of the surface spinor are:

$$\begin{bmatrix} u(r) \\ v(r) \end{bmatrix} = Cr^{\rho} \begin{bmatrix} J_{\nu_{j+}}(kr) \\ J_{\nu_{j-}}(kr) \end{bmatrix}, \tag{4.23}$$

C is a normalization constant, $\rho = -\frac{1}{2a}$ and $\nu_{j\pm}^2 = \lambda_{j\pm}^2 + \frac{1}{4a^2} = \left[\frac{1}{a}(j+\frac{1}{2}) \pm \frac{1}{2}\right]^2$.

To fully characterize the surface states and also be able to explore some more details of the system, we need to find the normalization constant C. It can be done noting that

$$\int (|u(r)|^2 + |v(r)|^2) ar\, dr\, d\phi = 1 \quad , \tag{4.24}$$

and substitution of equation (4.23) leads to

$$2C^2a\pi \int_0^R r^{2\rho+1}\left[J_{\nu_{j+}}(kr)^2 + J_{\nu_{j-}}(kr)^2\right]dr = 1 \quad . \tag{4.25}$$

To the leading order, the asymptotic expansion of the Bessel functions at large arguments [36] results in $J_{\nu_{j+}}(kr)^2 + J_{\nu_{j-}}(kr)^2 \to \frac{2}{\pi kr}$, and with a straightforward procedure we get to

$$C^2 = \frac{k}{4aR^{\frac{1}{a}+1}} \quad . \tag{4.26}$$

Some comments can be made about the normalization condition. In order to ensure normalizability at small arguments of the Bessel function for positive energies, i.e, $\nu_{j\pm} = +\left[\frac{1}{a}(j+\frac{1}{2}) \pm \frac{1}{2}\right]$, we must impose a condition on the values of j. Since $J_v(z) \to \infty$ as $z \to 0$ for $v < 0$ if v is non-integer (which is the case here), we must pick only non-negative values of j. On the other hand, for the negative energies, $\nu_{j\pm} = -\left[\frac{1}{a}(j+\frac{1}{2}) \pm \frac{1}{2}\right]$ we must pick only negative values for j.

In order to study the states near the singularity of the cone, we can use the expansion of the Bessel functions for small values of r and follow the development in reference [41] for the graphene analogue of our cone. Basically, with the asymptotic expansion of the Bessel functions in hands, we see that the local (near the apex) density of states behaves as:

$$D(E,r) \approx E^{(2\nu_{j_+}+1)} + E^{(2\nu_{j_-}+1)} \quad . \tag{4.27}$$

Since the values of $\nu_{j\pm}$ for the same angular momentum value, i.e, the same j, depends on the apex angle (recall that $\nu_{j\pm} = \left[\frac{1}{a}(j+\frac{1}{2}) \pm \frac{1}{2}\right]$), we can control the local density of states (and so the electronic and transport properties) just by manipulating the geometrical nature of the cone.

Now, the specification of a finite radius on the cone is equivalent to impose that there is no outward fermionic flux in the limits of the dot, i.e, $\alpha_+(R,\phi) + ie^{-i\phi}\alpha_-(R,\phi) = 0$, which leads to

$$J_{\nu_{j+}}(kR) - J_{\nu_{j-}}(kR) = 0 \quad . \tag{4.28}$$

From the boundary condition above we find the restriction $k = \frac{\zeta_{j,n}}{R}$, where $\zeta_{j,n}$ is the nth zero of $J_{\nu_{j+}}(z) - J_{\nu_{j-}}(z)$. Thus, the allowed positive energies become

$$E_{j,n} = A\frac{\zeta_{j,n}}{R} = \text{ where } j \in \mathbb{Z} \ , n \in \mathbb{N} \quad . \tag{4.29}$$

The identification of the finiteness of the cone naturally yielded discrete energies, printing the quantum confinement signature. Also, the geometrical parameter is intrinsic

in the energies since it is present on the $v_{j\pm}$ terms.

If we were to solve the Dirac equation with the $\frac{ib}{a^2r^2}$ term, we would get a Bessel-like radial equation for each component of the spinor in the same way we did, but our complete wavefunctions would be combinations of gamma functions, r power law functions and the Bessel functions. The same method of finding the roots of the Bessel functions would be applied, but it would be a lot harder to deal with the geometrical terms to show the influence of the apex angle in the results, so this is why we opted to not consider the renormalization term.

In can be instructive to see how the energies are affected by the geometry. In the following, we compare four different cones, with apex angles $\frac{\pi}{12}$, $\frac{\pi}{6}$, $\frac{\pi}{4}$ and $\frac{\pi}{3}$, for the ground and first excited states. We set $R = 1$, so that the quantity responsible for the confinement will be the apex angle. Intuitively, the energy must be higher for small apex angle, since this represents, from a Uncertainty Principle point of view, a stronger confinement.

Figure 4.1: Comparison between $\frac{\pi}{12}$, $\frac{\pi}{6}$ cones.

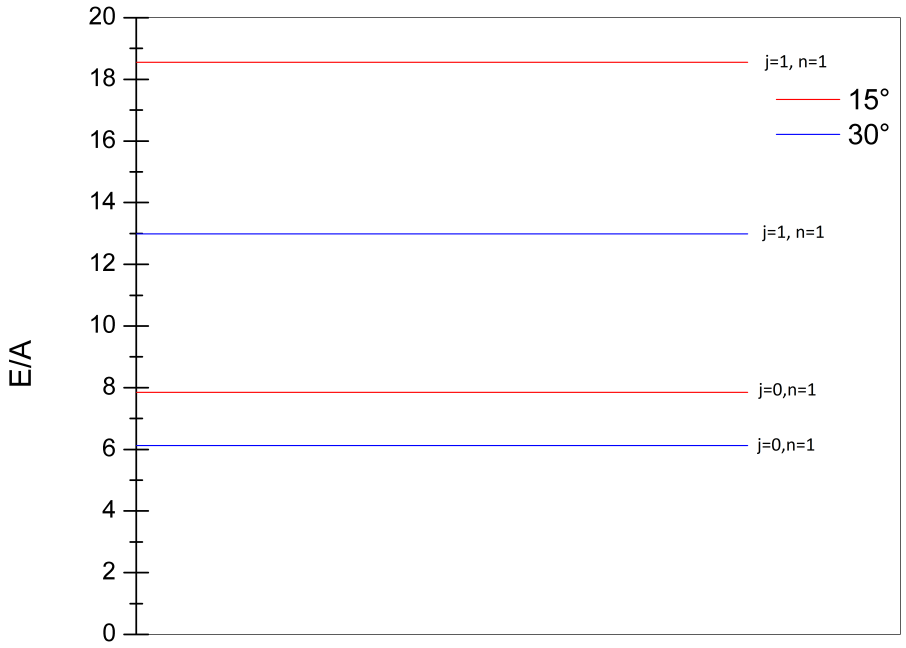

Figure 4.2: Comparison between $\frac{\pi}{4}$, $\frac{\pi}{3}$ cones.

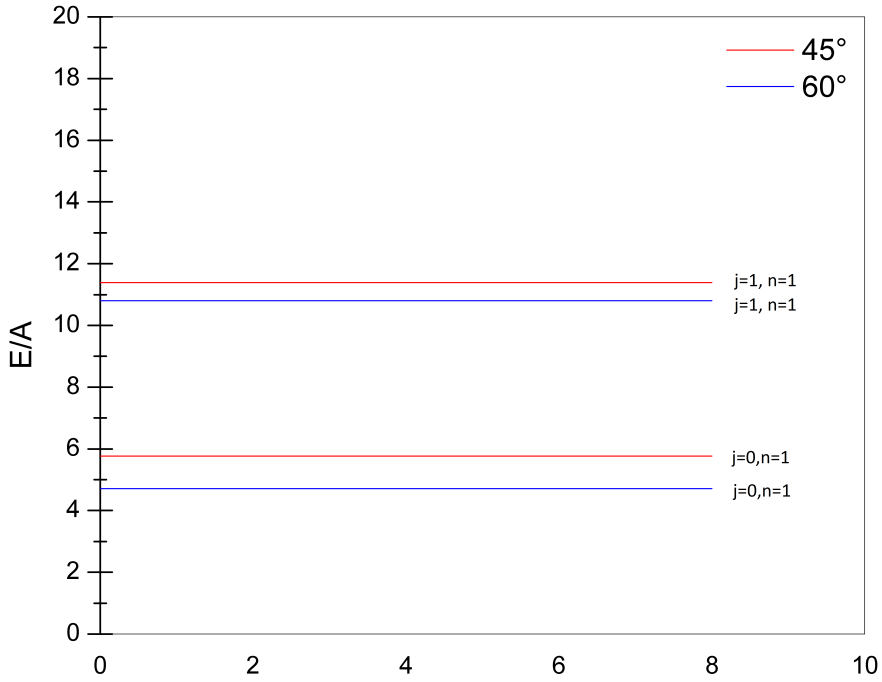

4.3 Discussion, conclusion and perspectives

In summary, we considered a conical topological insulator and found the Dirac operator that acts effectively on the surface particles. Indeed, they are described by a Dirac-like equation for massless fermions, and this equation couples to the non-trivial geometry of the surface between spin-connection terms and renormalization terms that depend on the apex angle of the cone. The surface states and energies are completely modulated by this geometrical term. In fact, while the radial component of the operator is modified by a spin-connection term, the azimuthal component is modified by a "Aharanov-Bohm" potential, that arises due to the singularity in the curvature at the tip of the cone. This is in parallel with the gravitational Aharanov-Bohm effect, where a conical space-time generated by a point mass exhibits global effects due to the non-trivial curvature at the origin. Thus, a study on the conical topological insulator surface is analogous to a study on a massless fermion travelling on a point mass particle space-time.

The surface states and its energies were determined. Complete characterization of this problem can be important for applications in new devices. It is known that constriction systems can be useful for filtering particles and controlling interactions [41],[42]. From a Schrodinger's equation point of view, if we couple two cones by the tip, this constriction will act like a particle filter, selecting particles with certain angular momentum. If this

still holds for the Dirac equation, one can think on a device made of two conical topological insulators connected by the tip, and use it for spintronics since the spin control in topological insulators is remarkably easier than other materials, due to the spin-locking property. Also, since we can control the local density of states and the energies controlling the apex angle of the cone, we could couple completely different cones together to get more control on the filtering. One other possibility is to combine different conical-shaped materials through the tip. Thus, from a fundamental physics point of view (dirac fermions in curved space) to an application point of view we can propose some perspectives on this work.

Appendix A

Some basic preliminary concepts

A.1 Bloch's theorem

The study of the properties of solids led to the development of the so called band theory, which describes the electronic structure of materials. The band theory's main point is based on Bloch's theorem, which exploit the periodicity in the arrangement of atoms in a crystal and concludes that one can write the energy eigenstates as Bloch waves. Well, if we consider a Hamiltonian $H(\mathbf{r}) = H(\mathbf{r}+\mathbf{R})$ in a periodic potential with period $\mathbf{R}$ than we can define a translation operator in such a way that:

$$T_r f(\mathbf{r}) = f(\mathbf{r}+\mathbf{R}) \quad .$$

Say that $f(\mathbf{r}) = |\psi_{n,\mathbf{k}}(\mathbf{r})\rangle = e^{i\mathbf{k}\cdot\mathbf{r}}|u_{n,\mathbf{k}}(\mathbf{r})\rangle$, where $|u_{n,\mathbf{k}}(\mathbf{r})\rangle$ is a periodic function with the same period $\mathbf{R}$. Now, applying the translation operator:

$$T_r|\psi_{n,\mathbf{k}}(\mathbf{r})\rangle = e^{i\mathbf{k}\cdot(\mathbf{r}+\mathbf{R})}|u_{n,\mathbf{k}}(\mathbf{r}+\mathbf{R})\rangle \quad . \tag{A.1}$$

Since $|u_{n,\mathbf{k}}(\mathbf{r}+\mathbf{R})\rangle = |u_{n,\mathbf{k}}(\mathbf{r})\rangle$, we have

$$\begin{aligned} T_r|\psi_{n,\mathbf{k}}(\mathbf{r})\rangle &= e^{i\mathbf{k}\cdot\mathbf{R}}e^{i\mathbf{k}\cdot\mathbf{r}}|u_{n,\mathbf{k}}(\mathbf{r})\rangle \\ &= e^{i\mathbf{k}\cdot\mathbf{R}}|\psi_{n,\mathbf{k}}(\mathbf{r})\rangle \quad . \end{aligned}$$

So, $|\psi_{n,\mathbf{k}}(\mathbf{r})\rangle$ is an eigenfunction of the translation operator with eigenvalue $e^{i\mathbf{k}\cdot\mathbf{R}}$. Well, the Hamiltonian is invariant under the translation operator, so $[H, T_r] = 0$, thus we see that the functions $|\psi_{n,\mathbf{k}}(\mathbf{r})\rangle$ are simultaneous eigenfunctions of T_r and H. That being

said, any eigenfunction of the Hamiltonian can be written as a linear combination of the functions $e^{i\mathbf{k}\cdot\mathbf{r}}|u_{n,\mathbf{k}}(\mathbf{r})\rangle$, where $|u_{n,\mathbf{k}}(\mathbf{r})\rangle$ are the Bloch waves.

If one write $H(\mathbf{k}) = e^{-i\mathbf{k}\cdot\mathbf{r}}H(\mathbf{r})e^{i\mathbf{k}\cdot\mathbf{r}}$, the eigenvalue equation for the energy is obtained:

$$H(\mathbf{k})|u_{n,\mathbf{k}}(\mathbf{r})\rangle = E_{n,\mathbf{k}}|u_{n,\mathbf{k}}(\mathbf{r})\rangle \quad . \tag{A.2}$$

The Hamiltonian eigenvalues $E_{n,\mathbf{k}}$ define the energy bands, and consequently the crystal band structure. Here "n" is an index that distinguishes the energy bands. Each electronic state characterized by n and k may be occupied by two electrons (one with spin up, the other with spin down). Electrons will naturally fill the lower energy states first to form the Fermi sea and the highest energy level of the occupied states is called the Fermi level. Around the Fermi level, if the band is partially occupied, we have a metallic state. Otherwise, if the band is fully filled, and there is an energy gap between the valence band and the conduction band, we have an insulating (for an energy gap larger than 4eV in general) state or a semiconducting (for an energy gap smaller than 4eV) state.

A.2 Berry's phase

One very interesting concept in quantum mechanics that will be useful in the next chapters is the concept of geometrical phase, or simply Berry's phase. It is well known that wave functions in general are defined up to a phase, so for example the equation (A.2) is invariant under the transformation $|u_{n,\mathbf{k}}(\mathbf{r})\rangle \rightarrow e^{i\phi(\mathbf{k})}|u_{n,\mathbf{k}}(\mathbf{r})\rangle$. We say that the eigenenergies, as observables must be, are gauge invariant.

Consider a Hamiltonian that is function of a set of arbitrary parameters represented as $\mathbf{R}$ and that it varies with time through this parameter $\mathbf{R} \rightarrow \mathbf{R(t)}$. We are interested in the time-evolution as $\mathbf{R}$ evolves in the parameter space along a path $\mathcal{C}$, considering that, at first, the system is in the state $|u_n(\mathbf{R}(t=0)\rangle$, that is solution to the equation

$$H(\mathbf{R}(t))|u_n(\mathbf{R}(t=0)\rangle = E_n(\mathbf{R}(t=0))|u_n(\mathbf{R}(t=0))\rangle \quad . \tag{A.3}$$

According to the adiabatic theorem, for a slowly (adiabatic) varying Hamiltonian, a system initially in one eigenstate will always remain in this instantaneous eigenstate (with

the parameter evolving in time). So, with slowly varying parameter, we have after some time t: $|u_n(\mathbf{R}(t=0)\rangle \to |u_n(\mathbf{R}(t)\rangle$. It was said that the adding of a phase does not change the observables, so we write a general quantum state related to the eigenstate as $|\psi(t)\rangle = e^{i\phi(t)}|u(\mathbf{R}(t))\rangle$, and the equation ruling the dynamics is

$$H(\mathbf{R}(t))|\psi(t)\rangle = i\hbar\frac{d}{dt}|\psi(t)\rangle \quad . \tag{A.4}$$

Now, from this equation one can obtain the phase factor to be the sum of the dynamical phase (that is related to the time evolution of the Hamiltonian) and a geometrical phase:

$$\phi(t) = \frac{1}{\hbar}\int_0^t E_n(\mathbf{R}t')dt' - i\int_0^t \langle u_n(\mathbf{R}(t'))|\frac{d}{dt'}|u_n(\mathbf{R}(t'))\rangle dt' \quad , \tag{A.5}$$

with $\gamma_c = i\int_0^t \langle u_n(\mathbf{R}(t'))|\frac{d}{dt'}|u_n(\mathbf{R}(t'))\rangle dt'$ being the geometrical phase. Its origin is related to the changes in the eigenkets by time evolution (not only the eigenenergies time-evolve), and it is path-dependent in the parameter space. To see that, let us rewrite γ_c as

$$\begin{aligned}\gamma_c &= i\int_0^t \langle u_n(\mathbf{R}(t'))|\nabla_{\mathbf{R}}|u_n(\mathbf{R}(t'))\rangle \cdot \frac{d\mathbf{R}}{dt'}dt' \\ &= i\int_{\mathbf{R}_0}^{\mathbf{R}_t} \langle u_n(\mathbf{R})|\nabla_{\mathbf{R}}|u_n(\mathbf{R})\rangle \cdot d\mathbf{R} \quad .\end{aligned}$$

Defining the Berry potential (or Berry connection) $\mathbf{A}_n(\mathbf{R}) = i\langle u_n(\mathbf{R})|\nabla_{\mathbf{R}}|u_n(\mathbf{R})\rangle$, the geometric phase is

$$\gamma_c = \int_{\mathbf{R}_0}^{\mathbf{R}_t} \mathbf{A}_n(\mathbf{R}) \cdot d\mathbf{R} \quad . \tag{A.6}$$

From the equation above, it is clear the dependence of the γ_c phase on the path. Also, we see that the Berry potential isn't gauge independent at first since under a transformation $|u_n(\mathbf{R})\rangle \to e^{i\lambda(\mathbf{R})}|u_n(\mathbf{R})\rangle$ and $\mathbf{A}_n(\mathbf{R}) \to \mathbf{A}_n(\mathbf{R}) - \nabla_R\lambda(\mathbf{R})$. The change in the geometric phase is $-\int_{\mathcal{C}} \nabla_R\lambda(\mathbf{R})d\mathbf{R} = \lambda(\mathbf{R}_0) - \lambda(\mathbf{R}_t)$. Now, if the path $\mathcal{C}$ in the parameter space is closed this is a gauge invariant phase and it is called the Berry phase. In mathematical terms,

$$\gamma_c = \oint_{\mathcal{C}} \mathbf{A}_n(\mathbf{R}) \cdot d\mathbf{R} \quad . \tag{A.7}$$

From an Ahanorov-Bohm experiment point of view, the Berry phase plays the role of the magnetic flux, and one can define the analogue of the magnetic field as $\mathbf{F} = \nabla \times \mathbf{A}_n$. This

is called the Berry curvature and its gauge-invariant form is

$$\mathbf{F} = i \sum_{m \neq n} \frac{\langle u_n(\mathbf{R}) | \nabla_{\mathbf{R}} H(\mathbf{R}) | u_m(\mathbf{R}) \rangle \times \langle u_m(\mathbf{R}) | \nabla_{\mathbf{R}} H(\mathbf{R}) | u_n(\mathbf{R}) \rangle}{(E_n - E_m)^2} \quad . \tag{A.8}$$

Finally, we can also write the Berry phase as (via Stokes' theorem)

$$\gamma_c = \int_{\mathcal{S}} \mathbf{F} \cdot d\mathbf{S} \quad . \tag{A.9}$$

A.3 Time-reversal symmetry and Kramers' theorem

A key concept on understanding topological properties of condensed matter systems is the concept of time-reversal symmetry. It is an operation (defined as $\mathcal{T}$) that inverts time in the following manner: $t \to -t$. If the Hamiltonian is $\mathcal{T}$ symmetric, so $[H, \Theta] = 0$, where

$$\Theta = K, \text{ for bosons} \tag{A.10}$$

$$\Theta = -i\sigma_y K, \text{ for fermions} \quad . \tag{A.11}$$

The operator Θ is known as the time reversal (anti-unitary) operator and K is the complex conjugation operator. The difference between the bosonic and fermionic $\mathcal{T}$ operators is due to the fact that spin-$\frac{1}{2}$ particles acquire additional rotation of their spin by π when making a complete round over the axis (here we chose y as the axis of rotation). Since we need a 4π rotation to bring back a fermion to its initial configuration, it isn't difficult to see that, for those particles, $\Theta^2 = -1$. This lead to a important result called the Kramers' theorem: states that are eigenstates of a $\mathcal{T}$ symmetric Hamiltonian describing fermions are at least twofold degenerate. This can be shown by picking up a pair of arbitrary energy states ψ and ϕ. Now,

$$\langle \Theta\phi | \Theta\psi \rangle = \langle \psi | \phi \rangle = \langle \phi | \psi \rangle^* \quad . \tag{A.12}$$

Say that $|\phi\rangle = \Theta\psi\rangle$, so:

$$\langle\Theta\psi|\psi\rangle^* = \langle\Theta^2\psi|\Theta\psi\rangle \quad . \tag{A.13}$$

If $\Theta^2 = -1$, straightforward computation leads to $\langle\Theta\psi|\psi\rangle = 0$, i.e, for each energy eigenstate, there is a orthogonal time-reversed partner, which is also an energy eigenstate with the same energy (remember that $[H, \Theta] = 0$]). Some important consequences of this result will show up on the next chapters.

Appendix B

Topology and condensed matter

We are talking about the interplay between geometrical and topological features in materials on this dissertation, so naturally we shall talk a bit about topology and how it connects with physics.

Topology as a field of mathematics is the study of the properties of some space, that are preserved under continuous transformations. It consists on the following concept: two objects are topological equivalent, if they can be transformed into one another by a smooth transformation. Here, "smooth transformation" means that you are allowed to bend and stretch an object but not to tear it apart or glue different regions together. If one follow this rule, than all the geometric forms that you can make from a given object are topologically equivalent. For example, two-dimensional surfaces are classified by the number of holes they have (or simply their *genus*). So, based on that, we conclude that the disk and the sphere are topologically equivalent since by smoothly deforming the sphere, we can produce a disk out. This is not true for a torus, since we can't form it without making a hole on the sphere, and so the sphere and the torus aren't topologically equivalent. On the other hand, the torus and a coffee mug are equivalent since we can deform the torus smoothly into the mug (keeping the number of holes constant).

From an analytical point of view, the topology of a surface is described by the Gauss-Bonnet's theorem:

$$\int_M K dA = 4\pi(1-g) \quad , \tag{B.1}$$

where K is the Gaussian curvature of the objectt M (also called *manifold*). Putting the equation above into words, it says that apart from a constant term, the integral of a manifold's Gaussian curvature will result in $(1-g)$, where the genus g is a integer

representing the number of holes of this object. Small deformations on the surface of the manifold will leads to a change of its curvature locally, but, from equation (B.1), it is clear that when we integrate this changed curvature over the whole surface (provided that we performed a smooth deformation) the right side of the equation still remains the same. Thus, the genus g is known as a 'topological invariant'.

Figure B.1: Topological equivalence between a sphere and a disk and between a torus and a coffee mug: As so the sphere into the disk, the torus can be smoothly deformed into a mug without tearing apart or joining two regions together

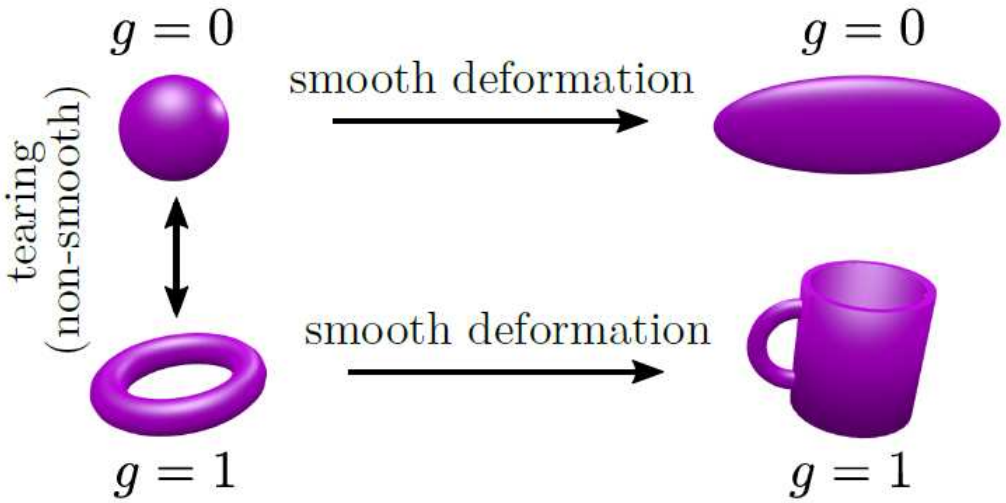

Source: Reference [21].

Long story short, from a mathematical point of view, topological classification focuses on fundamental distinctions between shapes and discards small details, being the connection by smooth deformation the fundamental concept for grouping objects on the same group. Bringing this ideas to physics, we can think about Hamiltonians describing many-particle systems with an energy gap between the ground ant excited states. Here the concept of smooth deformation is defined as an adiabatic change of some parameter (or the Hamiltonian itself) that does not close this energy gap. So, if we can connect two Hamiltonians by an adiabatic transformation they are topologically equivalents.

In order to clearly link the ideas from topology with physics and condensed matter, we will study a toy model that is a wonderful tool with so many features of topology and also of topological insulators. This model is named "the Su-Schrieffer-Heeger (SSH) model".

B.1 The Su-Schrieffer-Heeger (SSH) model

The Su-Schrieffer-Heeger (SSH) model is a tight-binding model that describes a single spin-less electron on a two site unit cell 1D lattice. It was proposed, in 1979, to describe the organic polymer polyacetylene: an atomic chain of carbon atoms with alternating single and double bonds. Basically there are N cells in the chain, each cell has two sites labelled A and B, where A corresponds to the dark circle and B to the white circle in the figure below:

Figure B.2: Ilustration of the SSH model. The dark circles are the sites A and the white circles are the sites B.

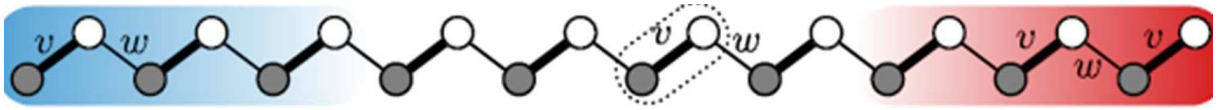

Source: Reference [11]

We set the lattice constant = 1 and neglect interactions between electrons, in a manner that the dynamics of each charge carrier is described by a single-particle Hamiltonian. As we can see in Figure B.2, the electrons can hop around from one site to another. The hopping amplitude within the unit cell is v, and the hopping amplitude that connects different (neighbours) unit cells is w. One can write the tight binding Hamiltonian as:

$$H = v\sum_n(|n,B\rangle\langle n,A| + h.c.) + w\sum_n(|n+1,A\rangle\langle n,B| + h.c.) \quad . \tag{B.2}$$

From a second quantization point of view, we write equation (B.2) as:

$$H = v\sum_n(A_n^\dagger B_n + B_n^\dagger A_n) + w\sum_n(A_{n+1}^\dagger B_n + B_{n+1}^\dagger A_n) + h.c \quad , \tag{B.3}$$

where where $A(B)_n^\dagger, A(B)_n$ are operators creating and annihilating, respectively, an electron on the A(B) sublattice at the n-th unit cell. At first we choose periodic boundary conditions, so we have translational invariance and it allows us to use the Fourier transform of the operators and write the momentum-space Hamiltonian:

$$H(k) = \begin{pmatrix} 0 & v + e^{ik}w \\ v + e^{-ik}w & 0 \end{pmatrix} \quad . \tag{B.4}$$

Straightforward diagonalization of this two dimensional matrix gives us the bulk dis-

persion relation:

$$E(k) = \pm\sqrt{v^2 + w^2 + 2vw\cos k} \quad . \tag{B.5}$$

From the energy dispersion, tt is clear that different choices of the parameters v and w will lead to different results. For example, if $v \neq w$ the dispersion is gapped and hence the system describe an insulator (that we'll call the trivial case for $v < w$ and the topological case for $v > w$) . Only in the case of v = w the gap closes and there are states available at arbitrary low energies above the Fermi level (which we have considered to be the zero energy level), therefore for $v = w$ the system describes a metal. This is ilustrated in the figure below:

Figure B.3: Dispersion relation obtained from bulk Hamiltonian for various v and w regimes.

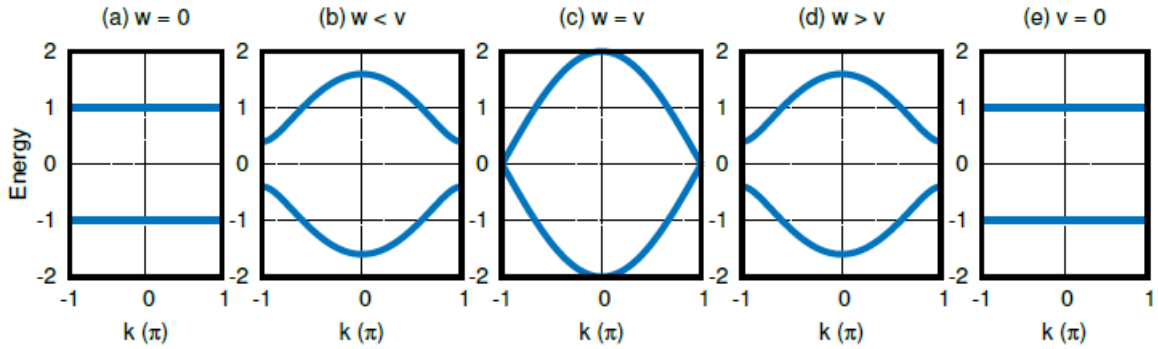

Source: Reference [17]

We can see that the change in the behavior of the system reminds us of a phase transition: there is some parameter that when changed, turn the system into an insulator (conductor). Despite the symmetric appearance about the $v = w$ case (it seems like the two insulator cases are the same), we have to look beyond the dispersion relation and study the eigenstates of the Hamiltonian to get a complete information about the three different cases above. In order to do so, we rewrite equation (B.4) as:

$$H(k) = \mathbf{h}(k) \cdot \boldsymbol{\sigma} \quad , \tag{B.6}$$

where $[\sigma_i]$ are the Pauli matrices and the vector $\mathbf{h}(k)$ is

$$h_x(k) = v + w\cos k;$$
$$h_y(k) = w\sin k;$$
$$h_z(k) = 0.$$

It is easy to find the eigenstates from equation (B.4) as

$$|\pm k\rangle = \begin{pmatrix} \pm e^{-i\phi(k)} \\ 1 \end{pmatrix} \quad , \tag{B.7}$$

where,

$$\phi(k) = \tan^{-1}\left(\frac{w\sin k}{v + w\cos k}\right) = \tan^{-1}\left(\frac{h_y(k)}{h_x(k)}\right) \quad . \tag{B.8}$$

If we make a h_x, h_y plot of the vector $\mathbf{h}(k)$ over a run into the first Brillouin zone, $k = -\pi \to \pi$, the path described will be a circle of radius w and centered at $(v, 0)$. In this plot, the structure of the eigenstates is described by the direction of the vector $\mathbf{h}(k)$, while the energy is given by its magnitude. Despite apparent symmetry in the energy dispersion equation (B.5), the plotted trajectories for the two insulator states ($v < w$ and $v > w$) are quite different, as we can see in the figure below:

Figure B.4: Trajectories of $\mathbf{h}(k)$ over a run into the first Brillouin zone for the three cases

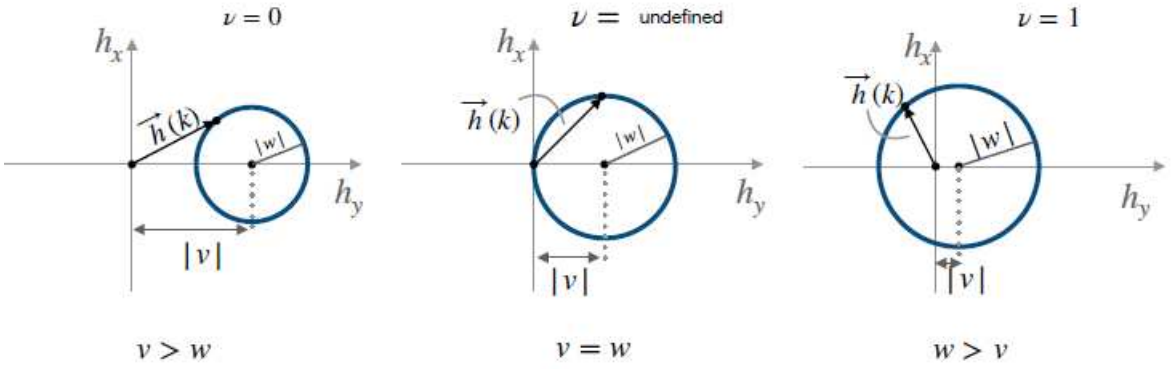

Source: Reference [17].

For the insulating cases of $v < w$, the trajectory of $\mathbf{h}(k)$ includes the origin and for the other cases with $v > w$ it does not. We can define than an integer ν that counts the number of times the loop winds around the origin in the (h_x, h_y) plane. For the two insulating states, this winding number is 0(1), while for the conductor ($v = w$) state the loop touches the origin and the winding number is undefined. In other words, the winding number distinguishes the two seemingly equivalent cases of insulators. Here lies the soul of what we call topology on condensed matter: the two insulator are distinct, and we can associate a number (that we can call a topological invariant) to each one. In order to connect them, we must run through a gap-less state (or a conductor state).

To show what topology has to do with it, we calculate the Berry potential as

$$A(k) = i\langle -k|\frac{d}{dk}|-k\rangle = -\frac{1}{2}\frac{d\phi}{dk} \quad .$$

We get a gauge-invariant result integrating this potential over the Brillouin zone:

$$-\frac{1}{\pi}\oint A(k)\,dk = \begin{cases} 1 & if\ v < w \\ 0 & if\ v > w \\ \text{undefined} & if\ v = w \end{cases} \quad . \tag{B.9}$$

A close look at this result tells us two things: this is a proper way to compute the winding number since the integral result is exactly the values of the winding number found by the trajectory plot earlier, and this is completely analogous to the Gauss-Bonnet's theorem discussed in the last section. The Berry potential is only a Stoke's theorem away of playing the analogous role of the curvature in Gauss-Bonnet's theorem (the Berry curvature does this job), while the Brillouin zone plays the part of the manifold. Thus, the role played by the genus is the same of the winding number. They are the topological invariants that defines the system, and, in order to connect two systems with different topology (say, to deform a sphere into a torus or to deform a trivial Hamiltonian into a topological Hamiltonian at the SSH model) we must have a topological phase transition (see Figure B.5), where the topological invariant changes. In the case of a manifold in the Gauss-Bonnet's theorem this corresponds to making a hole in the object, while in the SSH model this corresponds to closing the gap and accessing a conductor state.

Figure B.5: Ilustration of the phase diagram for the SSH model.

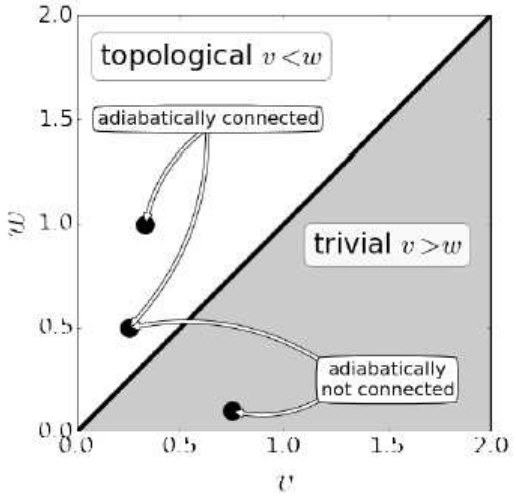

Source: Reference [11]

Although the SSH model isn't precisely a model for topological insulators, it gives us a good insight of the behaviour of the true ones: the bulk of a topological insulator has a winding number that is distinct from the vacuum winding number (we can think the vacuum like an insulator naturally), and so at the surface connecting the bulk and the vacuum lies a conducting state. More on this will be discussed on the next chapter.

B.1.1 Continuum model

In certain situations when the gap is really small or approximately zero, we can turn the lattice problem in a continuum problem. We have

$$H(k) = (v + w\cos k)\sigma_1 + \sigma_2 \sin k \quad . \tag{B.10}$$

The gap is zero when $H = 0$, i.e,

$$v + w\cos k = 0$$
$$w\sin k = 0.$$

Since v and w are positives, we must expand the hamiltonian over the $k = \pi$ point, where the identification $v = w$ closes the gap. This point is the so called Dirac point. Near the Dirac point,

$$k = \pi + k', \quad \cos k \approx -1, \quad \sin k \approx -k' \quad ,$$

and finally

$$H = (v-w)\sigma_1 - wk'\sigma_2 = m\sigma_1 - wk'\sigma_2, \text{ where } m = v-w \quad . \tag{B.11}$$

We can transform this Hamiltonian from momentum space to real space and get the following differential equation (here we choose w=1 without loss of generality, we are just re-scaling the energy):

$$i\hbar\sigma_2\frac{d\psi}{dx} + m\sigma_1\psi = E\psi \quad . \tag{B.12}$$

This is a first order differential equation in space, and structurally reminds us of the Dirac equation in one dimension. In fact, if we are exactly at the Dirac point, $v = w$ and $m = 0$, in a way that our Dirac-like equation turns out to be

$$i\hbar\sigma_2\frac{d\psi}{dx} = E\psi, \text{ with a dispersion relation } E(k') = \pm wk' \quad . \tag{B.13}$$

The equation above is analogous to that of a massless Dirac fermion in 1D. Because of this similarity we call it the massless Dirac Hamiltonian. Topological insulators are also described by massless Dirac Hamiltonians in the gap-less region. In fact the SSH model (and its generalizations) predicts a lot of others effects and behaviours that also appear on topological insulators, for example:

· Spin-charge separation

· Bulk-edge correspondence

· Number of Edge states as a topological invariant.

A more profound and complete discussion over all these features in the SSH model can be found on references [11], [12], [16].

B.2 Topological invariants and the bulk-edge correspondence

To continue the block building towards the topological materials, imagine a Bloch's Hamiltonian and let us define a topological invariant quantity $\mathcal{C}$ called Chern number:

$$\mathcal{C} = \frac{1}{2\pi}\int_{\mathcal{S}} \mathbf{F}\cdot d\mathbf{S} \quad , \tag{B.14}$$

where the surface $\mathcal{S}$ is a closed 2D space (such as a 2D Brillouin zone) and $\mathbf{F}$ is the Berry curvature. Note the similarity of the integral above with equation equation (B.1). In fact, the Chern number is a quantized integer (just like the genus), and being so, it must remain invariant under continuous transformations and it can be used to identify different topological phases: a system with a Chern number $\mathcal{C} = 0$ is said to be in a trivial phase, and a system with a Chern number $\mathcal{C} \neq 0$ is said to be in a topological phase (note the similarity with the winding number on the SSH model).

Bands with $\mathcal{C} \neq 0$ are called Chern bands. It is a straightforward procedure to show that it is only possible to have a non-zero Chern number only if time-reversal symmetry is broken [12]. For the $\mathcal{T}$ symmetric systems, $\Theta H(\mathbf{k})\Theta^{-1} = H(-\mathbf{k})$, and it is possible to classify the equivalence classes of Bloch Hamiltonians that can be deformed without closing the gap [13]. The $\mathcal{Z}_2$ invariant associated with this symmetry is defined through a unitary matrix $\omega_{mn}(\mathbf{k}) = \langle u_m(\mathbf{k})|\Theta|u_n(\mathbf{k})\rangle$, where the base functions for its construction are the occupied Bloch functions $|u_m(\mathbf{k})\rangle$.

We know that $\Theta^2 = -1$, so $\omega^T(\mathbf{k}) = -\omega(\mathbf{k})$. Now, there are some special Λ_a points in the BZ where $\mathbf{k} = -\mathbf{k}$, and we will show an example of them in a square lattice, where the Λ_a points are $k = 0$ and $\pm\frac{\pi}{a}$ along each axis:

Figure B.6: In 2D, the BZ has 4 special points. Due to $\mathcal{T}$ symmetry, only half of the BZ needs to be considered.

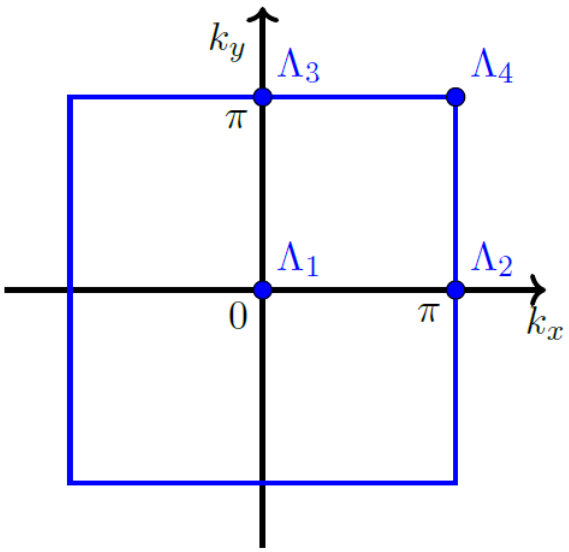

Source: Reference [16]

The matrix is antisymmetric at these special points. Now, the square root of the determinant of an antisymmetric matrix is known as the Pfaffian and we define a gauge-

invariant term as the

$$\delta_a = \frac{\mathrm{Pf}[\omega(\Lambda_a)]}{\sqrt{\det[\omega(\Lambda_a)]}} = \pm 1 \quad , \tag{B.15}$$

which we use to define the $\mathcal{Z}_2$ invariant as

$$(-1)^\nu = \prod_{a=1}^{4} \delta_a \quad , \tag{B.16}$$

where ν is the invariant we are looking for, and it can assume the values 0 and 1.

In general, additional symmetries simplifies the ν evaluation. For example, if one picks a crystal with spatial inversion ($\mathcal{I}$) symmetry, so $[H, \mathcal{P}] = 0$, with $\mathcal{P}$ being the parity operator. Thus, the Bloch eigenstates are also parity eigenstates at the special points in the BZ, with eigenvalue $\chi_m(\Lambda_a) = \pm 1$. The invariant in equation (B.16) is obtained identifying

$$\delta_a = \prod_m \chi_m(\Lambda_a) \quad . \tag{B.17}$$

For a spin symmetric system where, for example, S_z is conserved, independent Chern numbers $n_\uparrow$ and $n_\downarrow$ for spin up and down can be defined. Time-reversal symmetry dictates that $n_\uparrow + n_\downarrow = 0$ and with $n_\sigma = \frac{n_\uparrow - n_\downarrow}{2}$ the $\mathcal{Z}_2$ invariant is given by [13]

$$\nu = n_\sigma \bmod 2 \quad . \tag{B.18}$$

As a practical example of the classification based on the ν invariant, consider the edge band structure of a $\mathcal{T}$ symmetric two-dimensional insulator, illustrated in the Figure B.7. Since time-reversal symmetry is present, it is adequate to consider only half of the Brillouin zone $[0, \frac{\pi}{a}]$ because the other half will be just its mirror image. Depending on structural details of the Hamiltonian, there will be edge states inside the gap, and when it is the case, they are two-fold degenerate at the special $\Lambda = 0$ and $\Lambda = \frac{\pi}{a}$ points, as guaranteed by Kramers' theorem. Apart from these points, a spin-orbit interaction can break the degeneracy [14].

There are normally two ways to connect the states at $k_x = 0$ and the states at $k_x = \frac{\pi}{a}$. They can connect pairwise, as shown in Figure B.7(a), and for this case the bands touch the Fermi level an even number of times. In this specific situation, the edge states can be smoothly removed by pushing all of the bound states out of the energy gap. The other manner in which the states can connect, as can be seen in Figure B.7(b), is by an odd number of interceptions in the Fermi level. In contrast to the first situation, now the edge

states cannot be smoothly removed by driving parameters.

Figure B.7: The dispersion relation between two boundary degenerate points. a) An even number of states crossing the Fermi level is shown. b) An odd number of surface states crossing the Fermi level is shown.

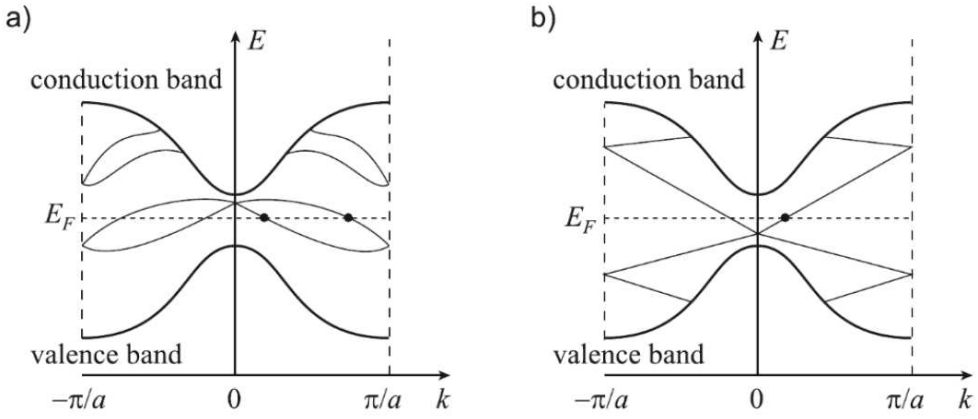

Source: Reference [30]

The two distinct cases illustrated in the figure above are characterized by the $\mathcal{Z}_2$ invariant ν. If the insulator has a even number of Kramers' pairs crossing the Fermi level, so the $\nu = 0$ and the insulator is in a trivial phase. Otherwise, if it has an odd number of Kramers' pairs crossing the Fermi level, $\nu = 1$ and it is in a topological phase. The principle guiding this result is the bulk-edge correspondence: it relates the number N_k of Kramers' pairs of edge states to the change of $\mathcal{Z}_2$ invariant at the boundary by [14]

$$N_k = \Delta\nu \text{ mod} 2 \quad . \tag{B.19}$$

In the next chapter we will return to these topics and hopefully they will become clearer.

Appendix C

Introduction to topological insulators

C.1 Integer quantum hall effect

The Integer quantum Hall effect (IQHE), discovered in 1980 by von Klitzing et al, was the first state of matter to be have an energy gap (just like an insulator) but not to be topologically equivalent to vacuum, exhibiting non-trivial transport properties. More specifically, one can measure a quantized Hall conductance in a 2DEG (two-dimensional electron gas) subjected to a strong and perpendicular magnetic field. In the magnetic field, the electrons form quantized Landau levels with a flat dispersion. At the edge, the confining potential pushes the Landau levels through the Fermi energy. For N filled Landau levels, one gets a Hall conductance of

$$\sigma_{xy} = N\frac{e^2}{h},\ N = 0, 1, 2, 3... \tag{C.1}$$

The Landau levels can be seen as energy bands for the electrons and if N Landau levels are filled, an energy gap separates the occupied and unoccupied states, as in an insulator. However, at the edges of the material the electrons have a different dynamics from those of the bulk. Since its orbits can't close, electrons move on skipping orbits along the edge (see Figure C.1). These skips at the edge lead to electronic states that propagate through the system edge. As the magnetic field determines the direction of motion of the electrons, the edge states are chiral (in the sense that they propagate in one direction only along the edge). No backscattering is allowed, as the edge state propagating in the opposite direction is located on the opposite side of the sample [15].

The existence of such "one way" edge states and the fundamental difference between

the quantum Hall state and the ordinary insulator is of topological nature. Basically, since the magnetic field breaks time-reversal symmetry, the topological invariant we look for is the Chern number. A famous result due to Thouless, Kohmoto, Nightingale, and den Nijs (TKNN) shows that the integer N in equation (C.1) is actually deeply connected with the Chern number. From a linear-response theory approach, they got [16]

$$\begin{aligned} \sigma_{xy} &= N\frac{e^2}{h} = \frac{e^2}{h}\frac{1}{2\pi}\int\int dk_x dk_y F_{xy}(\mathbf{k}), \\ F_{xy} &= \frac{\partial A_y(\mathbf{k})}{\partial k_x} - \frac{\partial A_x(\mathbf{k})}{\partial k_y}, \\ A_j &= i\sum_N \langle u_{n,\mathbf{k}}|\frac{\partial}{\partial k_j}|u_{n,\mathbf{k}}\rangle. \end{aligned} \tag{C.2}$$

In the equations above, A_j is the Berry potential for each of the N bands, F_{xy} is the Berry curvature and the integer N is precisely the sum over Chern numbers of the filled energy bands, as we can see from equation (B.14).

Figure C.1: Schematic illustration of the quantum Hall state. On the left we see the electronic orbits that are interrupted at the edges. On the right we see its band structure with a metallic edge state inside the bulk energy gap.

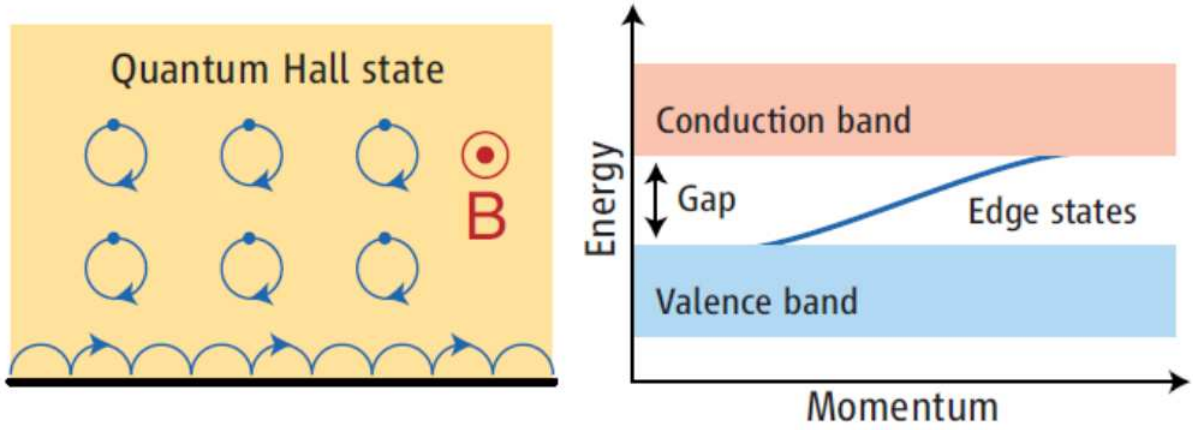

Source: Reference [31]

The IQHE is clearly topological, since for $N \neq 0$ it is a topological state by definition. Now, the edge states can be viewed, in the spirit of equation (B.19), from the bulk-edge correspondence. At a junction of a non-trivial material with finite Chern number and a trivial one with n = 0 (see Figure C.2), the difference $N_R - N_L$ in the number of right and left moving modes, is, (analogously to equation (B.19)) given by the difference ΔN

of the Chern numbers across the interface [16]:

$$N_R - N_L = \Delta N \quad . \tag{C.3}$$

For the topological invariant to change you need to close the gap at the interface, just like the SSH model.

Figure C.2: On the left we see the interface between two topologically distinct phases. On the right we see the edge band structure with a metallic state inside the bulk energy gap.

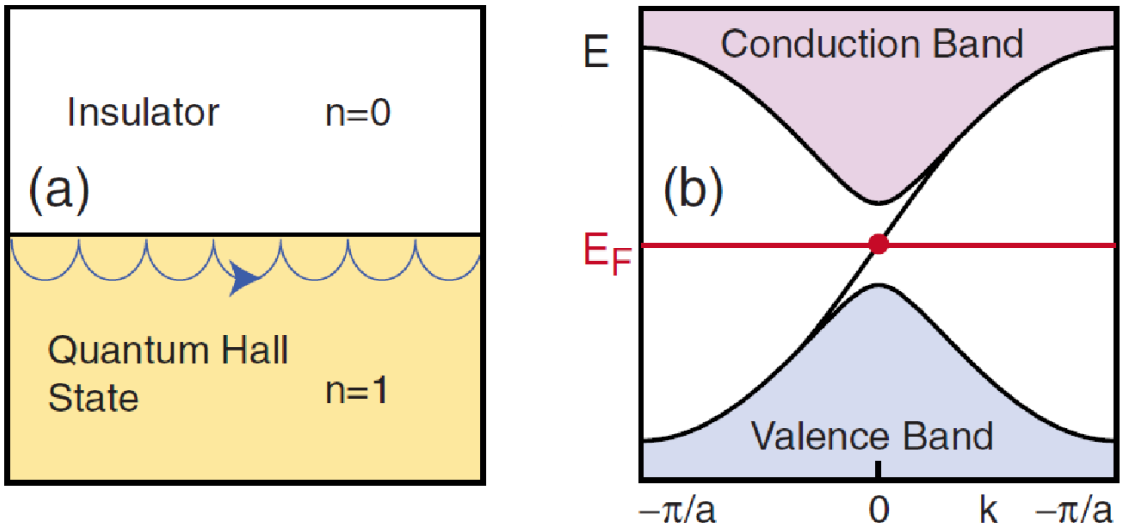

Source: Reference [32]

More on the quantum Hall effect, the TKNN result and the bulk-edge correspondence result, good references are [12],[13]. From now on we will discuss the $\mathcal{T}$ symmetric systems, and the so called Topological Insulators.

C.2 Quantum spin hall insulator - 2D Topological Insulators

Since the Hall conductivity (and hence the TKNN invariant) is not $\mathcal{T}$ symmetric, the topologically non-trivial states described in the preceding section can only occur when time-reversal symmetry is broken either by an external magnetic field or by magnetic

order. However, the spin-orbit interaction allows a different identification of insulating band structures topological classes when time-reversal symmetry is present.

A way of looking at such a $\mathcal{T}$ symmetric system is to make an overlay of two IQH systems with opposite spin, to form the quantum spin Hall insulator (QSHI). This gives a finite $\mathcal{Z}_2$ invariant according to equation (B.18). As in IQHE, in regions where the topological invariant changes (like as at the interface between QSHI and vacuum) there are conductors states (Figure C.3). Such states are called helical states. The Kramers' theorem ensures that these states come in counter-propagating doublets, with the spin-up state being the time-reversed partner of the other with spin down. Here the net charge current is 0 (and so is the Hall conductance), but since the two states are opposite spin-polarized there may be a net spin current (and so there is a spin Hall conductance). These counter-propagating states can not scatter into one another, and a way of understanding this is defining the states $|u_{k,\uparrow}\rangle = -\Theta|u_{-k,\downarrow}\rangle$, $|u_{-k,\downarrow}\rangle = \Theta|u_{-k,\uparrow}\rangle$ and taking the $\mathcal{T}$ symmetric scattering potential V with $\Theta V \Theta^{-1} = V$. So

$$\langle u_{k,\uparrow}|V|u_{-k,\downarrow}\rangle = 0 \quad , \tag{C.4}$$

showing that there is no overlap between the Kramers partners for scattering potentials that are time-reversal symmetric.

Figure C.3: Edge sates in QSHI. The left image interface between an EHQS in a different topological phase compared to vacuum. There are metallic edge states that are spin polarized with the left and right-oriented states connected by the time reversal symmetry. On the image at the right, there is a band structure scheme where the bulk gap and the spin-polarized edge metallic states are shown.

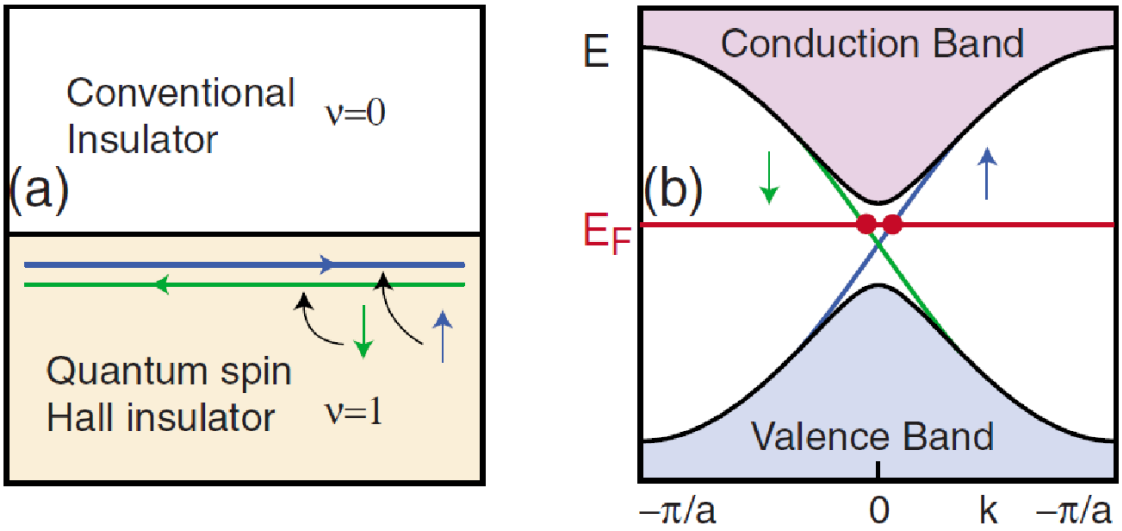

Source: Reference [31]

Graphene was the first QSH insulator [15]. Its topological properties results from spin-orbit coupling (SOC), which acts in a way as a $\mathcal{T}$ symmetric version of a external magnetic field. In graphene, the spin-orbit gap is very small, on the order of 10^{-6} eV, and because of this there is a practical difficulty on observing it experimentally. So we move for a different material with stronger SOC and apply these ideas. From theoretical investigations of the type III HgTe semiconductor quantum wells, it was shown that the topological insulating state should be realized in a regime, where the quantum well thickness d_{qw} is greater than a certain critical thickness d_c . The mechanism by which the topological insulator comes about is called band inversion and it was later shown to be generic [15]. The study of this system led to the development of the Bernevig-Hughes-Zhang model (BHZ model) for a HgTe/CdTe heterostructure.

Bernevig, Hughes and Zhang realized that the band structure for HgTe and CdTe are completely inverted across the Fermi level. In particular, the SOC split bands with Γ_8 and Γ_6 form conduction and valence bands in HgTe, while in CdTe they constitute valence and conduction. Through this mechanism, they derived a low-energy model that

describes a 2D QSHI (or a 2D topological insulator). The model is described by

$$H(k) = \epsilon(\mathbf{k}) \cdot \mathbf{1}_{4x4} + \begin{pmatrix} M_0(\mathbf{k}) & Ak_+ & 0 & 0 \\ Ak_- & -M_0(\mathbf{k}) & 0 & 0 \\ 0 & 0 & M_0(\mathbf{k}) & -Ak_- \\ 0 & 0 & -Ak_+ & -M_0(\mathbf{k}) \end{pmatrix}, \tag{C.5}$$

where $k_\pm = k_x \pm ik_y$, $\epsilon(\mathbf{k}) = C - D(k_x^2 + k_y^2)$, the effective mass is given by $M_0(\mathbf{k}) = M - B(k_x^2 + k_y^2)$ and the parameters A, B, C, D e M depend on the quantum well geometry. This is a four band model, which has two electron bands (spin up and spin down) and two hole bands (spin up and down). It has inversion symmetry, with electron and hole bands having opposite parity. The energies spectrum is

$$E_\pm = \epsilon(\mathbf{k}) \pm \sqrt{A^2(k_x^2 + k_y^2) + M_0^2(\mathbf{k})} \quad , \tag{C.6}$$

where the gap is $2M$ and the +(-) sign is associated with the conduction (valence) band.

Now, by looking to the energies (equation (C.6)) we can conclude that, for $\mathbf{k} = 0$ for example, the spectrum is gapped for $M > 0$ and $M < 0$, but is gapless for $M = 0$. In fact, one can calculate the topological invariant of each block of the BHZ Hamiltonian by equation (B.14), or by equation (B.16). The remarkable result is that the topological invariant is connected with the mass term on the BHZ Hamiltonian [15]. The $\mathcal{Z}_2$ invariant ν is 1 if $\frac{M}{B} > 0$ (we note that B is generally negative, and this is a topological phase), and it is zero if $\frac{M}{B} < 0$ (and this is a trivial phase). The change in the sign on the term $\frac{M}{B}$ is due the band-inversion mechanism: when there is band-inversion, the condition for the topological phase exists. In the figure below we keep all the parameters constant, except M, and illustrate the topological phase transition:

Figure C.4: On the left: $M = -1$, there is a gap and this is a topological insulating phase. On the center: $M = 0$, there is a gap closing, and this is the phase transition point. On the right: $M = -1$, there is a gap and this is a topological insulating phase.

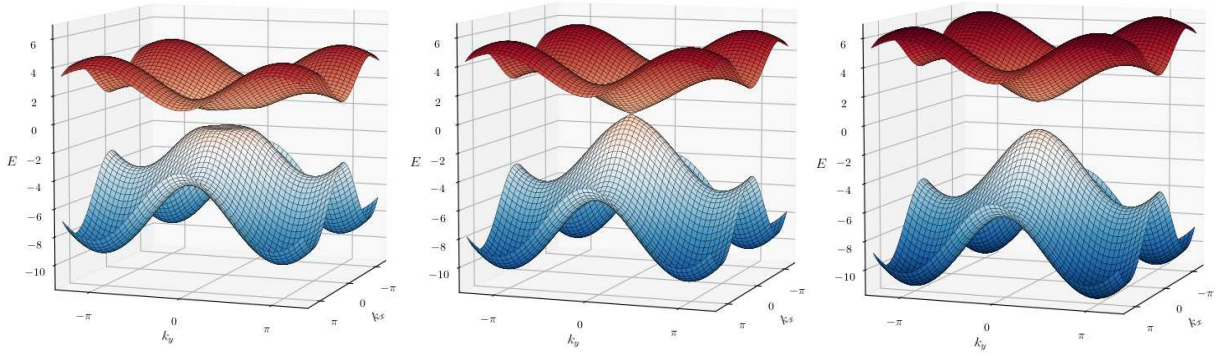

In the next section we will talk about the generalization of this model to three dimensions.

C.3 3D Topological Insulators

The discussion on the $\mathcal{Z}_2$ invariants and also the topological insulators can be generalized to three dimensions. On contrary to the 2D topological insulators, where there is an invariant ν that can assume two values that distinguishes the trivial insulators and the TI, in 3D TI there is a set of four $\mathcal{Z}_2$ topological invariant that can be used to classify the material: $(\nu_0;\nu_1\nu_2\nu_3)$, where ν_0 is called the strong index and he other three are the weak indices. Of the four topological invariants only ν_0 is robust in the presence of disorder, which leads to two distinct topological phases, with $\nu_0 = 0$ means trivial insulator while $\nu_0 = 1$ stands for topological insulator.

As in Section 3.2 for the 2D case,the 3D topological invariants $(\nu_0;\nu_1\nu_2\nu_3)$ can be understood based on bulk-edge correspondence. There are four points denoted by $\Gamma_{1,2,3,4}$ in the Brillouin zone of the surface of a 3D crystal that are $\mathcal{T}$ invariant and due to (see Figure B.6). These special degenerate points are points where the valence band touches the conduction band and here we will call them Dirac points, because of the linear dispersion relation on the special points neighbourhood. Analogous to the 2D case, the Fermi surface may circle an even or odd number of these points. When an even number of these points are surrounded, the material has $\nu_0 = 0$ and is a trivial insulator (see Figure C.5). But when the number of these points surrounded is odd, the material

has $\nu_0 = 1$ and is on a topological phase. Note the similarity with the discussion present in Section 3.2.

From a mathematical point of view, the strong topological invariant comes as a generalization of equation (B.16):

$$(-1)^{\nu_0} = \prod_{a=1}^{8} \delta_a \quad , \tag{C.7}$$

where now we account for the eight special points in the BZ of the material. Again, additional symmetries simplify the calculation, being the band-inversion symmetry, as we saw, the most important to our discussion. In fact, when parity symmetry is implied, we have

$$\delta_a = \prod_m \chi_m(\Gamma_a) \quad , \tag{C.8}$$

where the same arguments that led to equation (B.17) apply.

Figure C.5: In (a) is shown the surface of the TI. In (b) the BZ and the four $\mathcal{T}$ points $\Gamma_{1,2,3,4}$ are shown. Note that in (b) the Fermi surface surround only one of these points (thus, it is in a topological phase) and the respective Dirac cone is also shown. In (c) and (d) the band structure between two Kramers points is shown (note the similarity to Figure B.7).

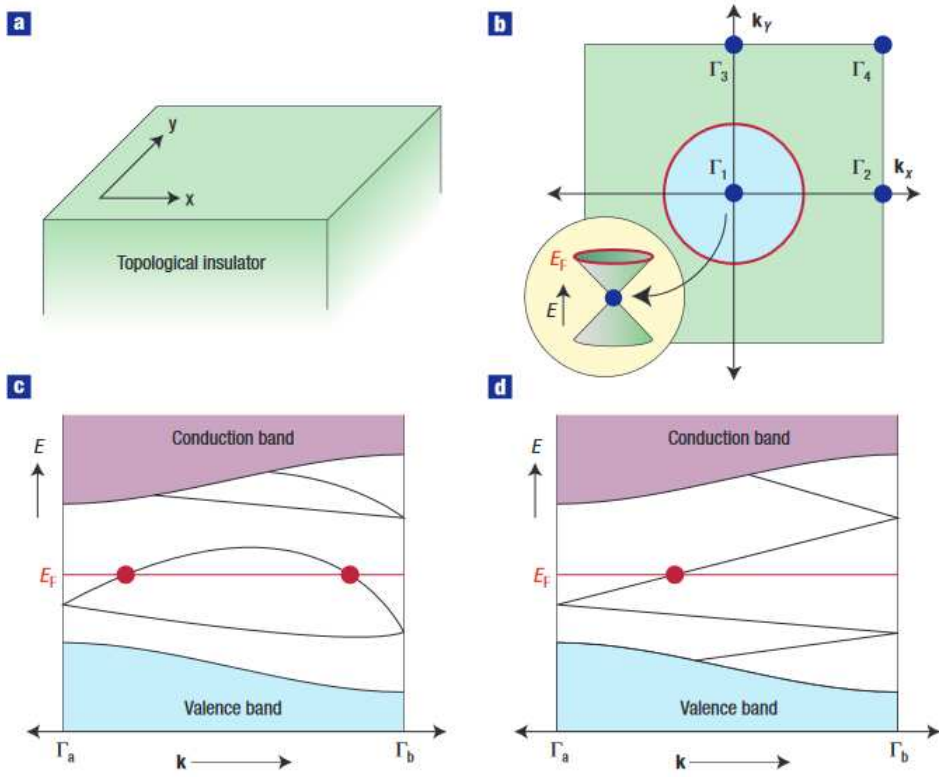

Source: Reference [33].)

The goal now is to generalize the BHZ model to three dimensions. In other to do so, one proceeding is to add a k_z-dependent term to the effective mass on the model (C.5),

and also to add a coupling for the two spin blocks in the matrix, since otherwise each block is undergoing a Chern insulator transition [13]. We arrive in a effective Hamiltonian, valid at low energies, which describe 3D topological insulators:

$$H(\mathbf{k}) = \epsilon(\mathbf{k}) \cdot \mathbf{1_{4x4}} + \begin{pmatrix} M(\mathbf{k}) & Ak_z + & 0 & \tilde{A}k_- \\ Ak_z & -M(\mathbf{k}) & \tilde{A}k_- & 0 \\ 0 & \tilde{A}k_+ & M(\mathbf{k}) & -Ak_z \\ \tilde{A}k_+ & 0 & -Ak_z & -M(\mathbf{k}) \end{pmatrix}, \tag{C.9}$$

where $M_0(\mathbf{k}) \rightarrow M(\mathbf{k}) = M - B(k_x^2 + k_y^2 + k_z^2)$. Again, all the parameters depend on the material geometry. This Hamiltonian is gapped at finite M, and a transition between the trivial and strong topological insulator phases is achieved by changing the sign of M, analogously to its 2D counterpart.

The properties of the edge states seen in the QSH (conductor state robust to non-magnetic impurities, absence of backscattering, opposite-spin propagating in opposite directions) are also present on the 3D TI. These states are protected by topology and always arise in regions where the strong topological invariant ν_0 changes, as in interface between a TI and the vacuum. To study them with can project the bulk Hamiltonian onto the surface of the material. Now, consider the TI surface at the x-y plane and the bulk in the $z < 0$ region. By projecting the Hamiltonian C.9 onto the surface, we get a surface operator described by the following Hamiltonian [5]:

$$H_{sur} = \tilde{A}(\sigma_x k_x + \sigma_y k_y) \quad . \tag{C.10}$$

The parameter $\tilde{A}$ is related to the Fermi velocity of the surface states. This surface Hamiltonian is valid in the simplest case, where there are only one Dirac point at the edge. We can write it on the real space as

$$H_{sur} = -i\hbar v_F \boldsymbol{\sigma} \cdot \boldsymbol{\nabla} \quad , \tag{C.11}$$

where the Pauli matrices are correlated to the actual spin of surface states. The Hamiltonian above is a massless Dirac-like Hamiltonian. Thus the surface states of the three-dimensional TI described by equation (C.11) have a linear spectrum. It can be shown also that for TI's the carriers in the surface states of topological insulator have their spin locked at a right angle to their momentum, which is a consequence of the strong SOC in

this materials [15]. This and the other features are illustrated below.

Figure C.6: Spin helical texture of surface states near the center of the Brillouin zone of a three-dimensional IT. On the left: The helicity of the states in the conduction band is opposite to that of the valence band states. On the right: The spin is locked to the surface at right angles to the momentum, and opposite momentum states have opposite spin.

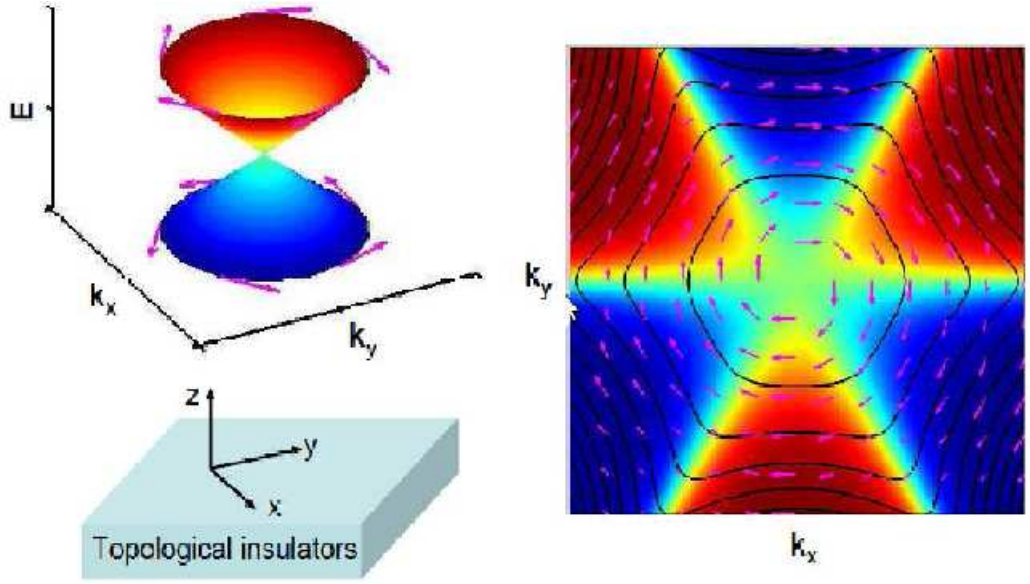

Source: Reference [34]

Appendix D

Effective BHZ surface Hamiltonian in conical coordinates

In reference [22], the authors developed an unified approach for the BHZ model in arbitrary curvilinear coordinates. We followed them towards the construction of the conical TI, and here we will identify the terms that produces the surface Hamiltonian.

Evaluation of the matrix elements

$$H_{suf} = \begin{bmatrix} \langle +|H_{\|}|+\rangle & \langle +|H_{\|}|-\rangle \\ \langle -|H_{\|}|+\rangle & \langle -|H_{\|}|-\rangle \end{bmatrix} \quad ,$$

leads to

$$H_{sur} = \begin{bmatrix} 0 & \mathcal{D}_+ \\ \mathcal{D}_- & 0 \end{bmatrix},$$

where

$$\mathcal{D}_+ = \sum_{i=1}^{2} \left[(\eta_i A - \xi_i m_2) \left(\partial_i + \frac{1}{2}[\partial_i \ln(\sqrt{G}] \right) + \frac{1}{2}[\partial_i (\eta_i A - \xi_i m_2)] \right],$$

$$\mathcal{D}_- = \sum_{i=1}^{2} \left[-(\eta_i A - \xi_i m_2)^* \left(\partial_i + \frac{1}{2}[\partial_i \ln(\sqrt{G}] \right) - \frac{1}{2}[\partial_i (\eta_i A - \xi_i m_2)^*] \right].$$

In the expressions above,

$$\eta_i = \frac{\langle \sqrt{G} \boldsymbol{\theta}_+^\dagger \sigma^i \boldsymbol{\theta}_- \rangle}{\langle \sqrt{G} \rangle} \quad ,$$

$$\xi_i = \sum_{j=1}^{2} \frac{\langle \sqrt{G} b_j^i \boldsymbol{\theta}_+^\dagger \sigma^i \boldsymbol{\theta}_- \rangle}{\langle \sqrt{G} \rangle} \quad .$$

All the averages here are taken with respect to the normal coordinate, i.e, θ and $b_j^i =$

$\partial_j \boldsymbol{e}_3) \cdot \boldsymbol{e}^i$. Also, $\boldsymbol{\theta}_+$ and $\boldsymbol{\theta}_-$ are defined in equations 4.11 and 4.12. So, we can evaluate all necessary terms.

$$b_1^1 = b_2^1 = b_1^2 = 0, \text{ while } b_2^2 = \frac{b}{ar} \quad ,$$

$$\boldsymbol{\theta}_+^\dagger \sigma^1 \boldsymbol{\theta}_- = -1 \quad ,$$

$$\boldsymbol{\theta}_+^\dagger \sigma^2 \boldsymbol{\theta}_- = \frac{i}{ar} \quad .$$

Since all the averages are over the normal component, and it is reasonable to assume that the θ coordinate will be practically constant at the surface, we can drop the averages and we get

$$\eta_1 = -1 \quad ,$$
$$\eta_2 = \frac{i}{ar} \quad ,$$
$$\xi_1 = 0 \quad ,$$
$$\xi_2 = \frac{ib}{a^2 r^2} \quad .$$

Substituting this quantities on the effective Dirac operator, we arrive in the conical Dirac operator for a topological insulator:

$$\mathcal{D}_\pm = \mp A \left(\frac{\partial}{\partial r} + \frac{1}{2r} \right) + \left(\frac{iA}{ar} + \frac{ib}{a^2 r^2} m_2 \right) \frac{\partial}{\partial \phi}.$$

References

[1] ANDERSON, Philip W. **More is different**. Science, v. 177, n. 4047, p. 393-396, 1972.

[2] FRASER, Gordon (Ed.). **The New Physics: For the Twenty-First Century**. Cambridge University Press, 2006.

[3] FONSECA, J. M. **Algumas contribuições ao estudo do grafeno e dos isolantes topológicos**. Tese de doutorado. Departamento de Física, Universidade Federal de Viçosa, 2012.

[4] KLITZING, K. v; DORDA, Gerhard; PEPPER, Michael.**New method for high-accuracy determination of the fine-structure constant based on quantized Hall resistance**. Physical Review Letters, v. 45, n. 6, p. 494, 1980.

[5] QI, Xiao-Liang; ZHANG, Shou-Cheng. **Topological insulators and superconductors**. Reviews of Modern Physics, v. 83, n. 4, p. 1057, 2011.

[6] QI, Xiao-Liang; ZHANG, Shou-Cheng. **The quantum spin Hall effect and topological insulators**. arXiv:1001.1602, 2010.

[7] GOMEZ, Daniel E.; CALIFANO, Marco; MULVANEY, Paul. **Optical properties of single semiconductor nanocrystals**. Physical Chemistry Chemical Physics, v. 8, n. 43, p. 4989-5011, 2006.

[8] LINDER, Jacob; YOKOYAMA, Takehito; SUDBØ, Asle. **Anomalous finite size effects on surface states in the topological insulator Bi2Se3**. Physical review B, v. 80, n. 20, p. 205401, 2009.

[9] SIROKI, Gleb et al. **Protection of surface states in topological nanoparticles**. Physical Review Materials, v. 1, n. 2, p. 024201, 2017.

[10] LEE, Dung-Hai. **Surface states of topological insulators: The Dirac fermion in curved two-dimensional spaces**. Physical review letters, v. 103, n. 19, p. 196804, 2009.

[11] ASBÓTH, János K.; OROSZLÁNY, László; PÁLYI, András. **A short course on topological insulators**. Lecture notes in physics, v. 919, 2016.

[12] SHANKAR, R. **Topological insulators – a review**. arXiv:1804.06471, 2018.

[13] Shen, S.-Q. **Topological Insulators: Dirac Equation in Condensed Matters**. Springer, 2013.

[14] KANE, Charles L. **Topological Band Theory and the $\mathcal{Z}_2$ Invariant**. In: Contemporary Concepts of Condensed Matter Science. Elsevier, 2013. p. 3-34.

[15] BERNEVIG, B. Andrei; HUGHES, Taylor L. **Topological insulators and topological superconductors**. Princeton university press, 2013.

[16] JURGENS, Stefan. **Correlated Topological Materials**. Tese de doutorado. Julius-Maximilians-Universität of Wurzburg, 2017.

[17] BATRA, Navketan; SHEET, Goutam. **Understanding Basic Concepts of Topological Insulators Through Su-Schrieffer-Heeger (SSH) Model**. arXiv:1906.08435, 2019.

[18] IMURA, Ken-Ichiro et al. **Spherical topological insulator**. Physical Review B, v. 86, n. 23, p. 235119, 2012.

[19] RIDER, Marie S. et al. **A perspective on topological nanophotonics: Current status and future challenges**. Journal of Applied Physics, v. 125, n. 12, p. 120901, 2019.

[20] SIROKI, G. et al. **Single-electron induced surface plasmons on a topological nanoparticle**. Nature communications, v. 7, p. 12375, 2016.

[21] CANDIDO, Denis Ricardo. **Blurring the boundaries between topological and non-topological physical phenomena in dots**. Tese de Doutorado. Universidade de São Paulo, 2018.

[22] TAKANE, Yositake; IMURA, Ken-Ichiro. **Unified description of Dirac electrons on a curved surface of topological insulators**. Journal of the Physical Society of Japan, v. 82, n. 7, p. 074712, 2013.

[23] BRANDT, F. T.; SÁNCHEZ-MONROY, J. A. **Dirac equation on a curved surface**. Physics Letters A, v. 380, n. 38, p. 3036-3043, 2016.

[24] DE SOUSA GERBERT, Ph; JACKIW, R. **Classical and quantum scattering on a spinning cone**. Communications in Mathematical Physics, v. 124, n. 2, p. 229-260, 1989.

[25] FONSECA, Jakson M. et al. **Berry phases and zero-modes in toroidal topological insulator**. The European Physical Journal B, v. 89, n. 6, p. 153, 2016.

[26] FONSECA, Jakson M.; MOURA-MELO, Winder A.; PEREIRA, Afranio R. **Geometrically induced electric polarization in conical topological insulators**. Journal of Applied Physics, v. 111, n. 6, p. 064913, 2012.

[27] RIDER, Marie S. et al. **Experimental signature of a topological quantum dot**. arXiv:1905.06193, 2019.

[28] SHAN, Wen-Yu; LU, Hai-Zhou; SHEN, Shun-Qing. **Effective continuous model for surface states and thin films of three-dimensional topological insulators**. New Journal of Physics, v. 12, n. 4, p. 043048, 2010.

[29] HASAN, M. Zahid; MOORE, Joel E. **Three-dimensional topological insulators**. Annu. Rev. Condens. Matter Phys., v. 2, n. 1, p. 55-78, 2011.

[30] JACAK, Janusz; GONCZAREK, Ryszard; JACAK, Lucjan. **Application of braid groups in 2D Hall system physics: composite Fermion structure**. World Scientific, 2012.

[31] KANE, Charles; MOORE, Joel. **Topological insulators**. Physics World, v. 24, n. 02, p. 32, 2011.

[32] HASAN, M. Zahid; KANE, Charles L. **Colloquium: topological insulators**. Reviews of modern physics, v. 82, n. 4, p. 3045, 2010.

[33] KANE, Charles L. **Condensed matter: An insulator with a twist**. Nature Physics, v. 4, n. 5, p. 348, 2008.

[34] LIU, Chao-Xing et al. **Model Hamiltonian for topological insulators**. Physical Review B, v. 82, n. 4, p. 045122, 2010.

[35] FILGUEIRAS, C.; SILVA, E. O.; ANDRADE, F. M. **Nonrelativistic quantum dynamics on a cone with and without a constraining potential**. Journal of Mathematical Physics, v. 53, n. 12, p. 122106, 2012.

[36] SEKELJIC, Nada. **Asymptotic expansion of Bessel functions; applications to electromagnetics**. Dynamics at the Horsetooth, v. 2, 2010.

[37] LAMMERT, Paul E.; CRESPI, Vincent H. **Graphene cones: Classification by fictitious flux and electronic properties**. Physical Review B, v. 69, n. 3, p. 035406, 2004.

[38] OSIPOV, Vladimir Andreevich; KOCHETOV, Evgenii Andreevich. **Dirac fermions on graphite cones**. Journal of Experimental and Theoretical Physics Letters, v. 73, n. 10, p. 562-565, 2001.

[39] BEZERRA, Valdir Barbosa. **On some classical and quantum effects due to gravitational fields**. Brazilian journal of physics, v. 36, n. 1B, p. 141-156, 2006.

[40] FERREIRA, Diego L. et al. **Size-dependent bandgap and particle size distribution of colloidal semiconductor nanocrystals**. The Journal of chemical physics, v. 147, n. 15, p. 154102, 2017.

[41] GOMES, Felipe Azevedo et al. **Electronic properties of single and double napped carbon nanocones**. The European Physical Journal B, v. 92, n. 2, p. 41, 2019.

[42] KOWALSKI, K.; REMBIELIŃSKI, J. **On the dynamics of a particle on a cone**. Annals of Physics, v. 329, p. 146-157, 2013.

[43] DEZHKAM, M.; ZAKERY, A. **Exact investigation of the electronic structure and the linear and nonlinear optical properties of conical quantum dots**. Chinese Optics Letters, v. 10, n. 12, p. 121901-121901, 2012.